Revista Mexicana de Astronomía y Astrofísica, **47**, 361–383 (2011)

THE NATURE AND ORIGIN OF NARROW LINE AGN ACTIVITY IN A SAMPLE OF ISOLATED SDSS GALAXIES

R. Coziol,[1] J. P. Torres-Papaqui,[1] I. Plauchu-Frayn,[2] J. M. Islas-Islas,[1]
R. A. Ortega-Minakata,[1] D. M. Neri-Larios,[1] and H. Andernach[1]

Received 2011 May 26; accepted 2011 August 1

RESUMEN

Discutimos la naturaleza y origen de la actividad nuclear observada en una muestra de 292 galaxias con líneas de emisión angostas del SDSS, cuya formación y evolución se considera que ha ocurrido en aislamiento. La fracción de galaxias con un núcleo activo (AGNs) o de objetos de transición (TOs; un AGN con formación estelar circunnuclear) alcanza 64% de la muestra. Verificamos que la probabilidad de que una galaxia muestre un núcleo activo aumenta con la masa de su bulbo (Torres-Papaqui et al. 2011). También encontramos evidencia de que dicha tendencia es realmente un subproducto de la morfología, y sugiere que el fenómeno AGN está íntimamente ligado al proceso de formación de galaxias. Los AGNs con líneas de emisión angostas en nuestra muestra son consistentes con una versión a menor escala o menor energía de cuásares y AGNs con líneas de emisión anchas.

ABSTRACT

We discuss the nature and origin of the nuclear activity observed in a sample of 292 SDSS narrow-emission-line galaxies, considered to have formed and evolved in isolation. The fraction of Narrow Line AGNs (NLAGNs) and Transition type Objects (TOs; a NLAGN with circumnuclear star formation) amounts to 64% of the galaxies. We verify that the probability for a galaxy to show an AGN characteristic increases with the bulge mass of the galaxy (Torres-Papaqui et al. 2011), and find evidence that this trend is really a by-product of the morphology, suggesting that the AGN phenomenon is intimately connected with the formation process of the galaxies. The NLAGNs in our sample are consistent with a scaled-down or powered-down versions of quasars and Broad Line AGNs.

Key Words: galaxies: active — galaxies: formation

1. INTRODUCTION

Spectroscopic surveys, like the Sloan Digital Sky Survey (SDSS) (York et al. 2000; Stoughton et al. 2002), have revealed that a large fraction of galaxies in the nearby universe show emission lines consistent with some kind of nuclear activity. Using diagnostic diagrams that compare various emission line ratios, different classification criteria were proposed to classify these galaxies based on the possible sources of excitation of the gas (Baldwin, Phillips, & Terlevich 1981; Veilleux & Osterbrock 1987; Kewley et al. 2001; Kauffmann et al. 2003). These classification criteria imply that there are two possible main sources: thermal sources, which are associated with star forming activity, and non-thermal sources, which are produced by the accretion of matter onto a Super-Massive Black Hole (SMBH) in the nucleus of the galaxies–the so called Active Galactic Nuclei (AGNs).

The majority of the emission line galaxies in the SDSS turn out to be star forming galaxies (SFGs). However, recent studies (e.g., Miller et al. 2003; Martínez et al. 2010; Torres-Papaqui et al. 2011) inferred that the actual number of galaxies with a non-thermal ionization source in their nucleus could be much higher than previously believed, but the evidence was somewhat obscured by the large variation of characteristics presented by AGNs. For ex-

[1]Departamento de Astronomía, Universidad de Guanajuato, Guanajuato, Mexico.
[2]Instituto de Astrofísica de Andalucía (CSIC), Granada, Spain.

ample, in the Seyfert 1, where we can distinguish broad emission line components akin to what is observed in quasars (Osterbrock 1989; Weedman 1986; Krolik 1999), the presence of a SMBH seems indubitable. However, a significantly larger fraction of AGNs show only narrow emission lines. Also, many researchers have alluded to different characteristics for these Narrow Line AGNs (NLAGNs) by separating them into two main groups, the high ionization galaxies, generally called Seyfert 2 (Sy2), and the low ionization ones, called LINERs, which stands for Low Ionization Nuclear Emission-line Regions (Heckman 1980; Coziol 1996; Kewley et al. 2006). As a consequence, the source of ionization of NLAGNs, although clearly distinct from SFGs, is still an actively debated subject, and there is presently no consensus about their nature or evolutionary status.

It is usually admitted that both Sy2 and LINERs are phenomena that occur in early-type (Sa and Sb) spiral galaxies in the field, that is, galaxies forming in relatively low galactic density environments (Heckman 1980). On the other hand, there is growing evidence that NLAGNs in clusters and compact groups of galaxies differ from those in the field by their earlier morphological types and intrinsic low luminosities (Phillips 1986; Coziol et al. 1998a; Miller et al. 2003; Wake et al. 2004; Martínez et al. 2008, 2010; Torres-Papaqui et al. 2011). These differences seem to point to distinct formation mechanisms for galaxies in different environments, which could have also affected the formation and evolution of their black holes. For example, the Low Luminosity AGNs (LLAGNs) found in compact groups and clusters of galaxies appear to prefer massive bulge spiral galaxies or elliptical galaxies–galaxies which are poor in gas–and it is this actual scarcity of matter that can be accreted that is assumed to explain the low luminosity of these objects (Martínez et al. 2008; Torres-Papaqui et al. 2011). This explanation is fully consistent with the starving quasar model (Richstone et al. 1998; Gavignaud et al. 2008; Martínez et al. 2008, 2010), according to which a SMBH that had accreted at high rates in the past, producing a quasar-like activity, evolved as its reservoir of gas was depleted into a slowly accreting SMBH producing a LLAGN.

In order to test the idea of a variation of the AGN phenomenon in different environments we considered important to study galaxies for which the influence of their environment was minimal. These are galaxies that are relatively isolated–that is, they formed in low galactic density environments and evolved without major interactions with other galaxies.

2. DESCRIPTION OF THE SAMPLE AND DATA USED FOR ANALYSIS

Our sample of isolated galaxies was selected from the 2 Micron Isolated Galaxies catalogue (hereafter 2MIG), as compiled by Karachentseva et al. (2010). The 2MIG catalogue contains 3227 galaxies, covering the entire sky. All the galaxies have a near-infrared magnitude brighter than $K_s = 12$, and a projected image that extends across an angular diameter $a_K \geq 30''$. The isolation criterion used in this catalogue is the following: a galaxy is considered isolated when its nearest neighbor has a size within a factor 4 of the major-axis diameter of the target galaxy, and lies more than 20 diameters away from it. This criterion assures that a galaxy with a typical diameter of 20 kpc and peculiar velocity of the order of 150 km s^{-1} was not influenced by a similar type of galaxy during the last $\sim$3 Gyr (Turner et al. 1979).

To produce our sample, we have cross-correlated the positions of the galaxies in the 2MIG catalogue with spectroscopic targets in the Sloan Digital Sky Survey Data Release 7 (SDSS DR7) database (Abazajian et al. 2009). This resulted in 445 galaxies, which represents 88% of the galaxies in the 2MIG catalogue covered by the SDSS DR7. The remaining 12% are galaxies for which spectroscopic data were not obtained by SDSS, because they were too nearby or too bright.

Color images of the galaxies were obtained using the tool CHART of SDSS[3]. After visual inspection, we eliminated 28 galaxies with morphological peculiarities or possible faint companions, in apparent contradiction with the isolation assumption.

A preliminary examination of the spectra reveals that all these galaxies except one show emission lines. The only non-emission “isolated” galaxy is identified as SDSS J072635.39+431746.8. This is a nearby galaxy, $z = 0.0105$, with a possible E or S0 morphology. Being the only galaxy of its kind it was excluded from our study.

Also excluded from our analysis were two extremely blue S0-like galaxies, with spectra typical of late-type spirals–showing a recent and extremely intense level of star formation. A careful examination of their images suggested that they are low mass irregular or morphologically peculiar galaxies. Their positions in the standard diagnostic diagram reveal that they are HII galaxies–small mass and low gas metallicity starburst galaxies (see Coziol 1996).

Only five galaxies in our sample were found to have broad emission line components. The spectra

[3]`http://cas.sdss.org/dr7/en/tools/chart/chart.asp`.

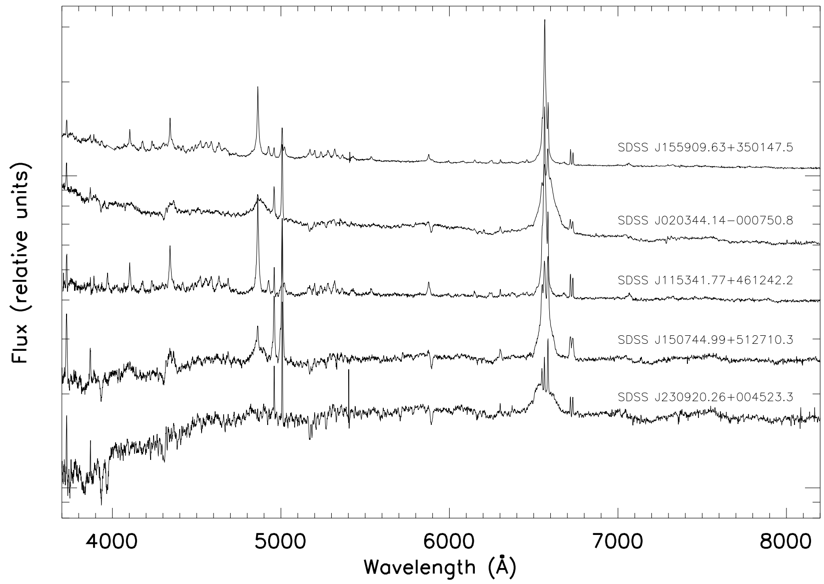

Fig. 1. Spectra of the broad line AGNs of our original sample of 2MIG galaxies. The flux scale is relative and was slightly displaced for clarity.

of these galaxies are presented in Figure 1. These galaxies were also discarded from our analysis.

We classified the 409 remaining galaxies as isolated Narrow Emission Lines Galaxies (NELGs). The spectra of these galaxies were subsequently corrected for Galactic extinction (Schlegel, Finkbeiner, & Davis 1998), shifted to their rest frame, resampled to $\Delta\lambda$=1 Å between 3400 and 8900 Å, and processed using the spectral synthesis code STARLIGHT (Cid Fernandes et al. 2005), which produces a stellar population template that fits the continuum of each galaxy. We ran STARLIGHT using a combination of $N_\star$ Simple Stellar Populations (SSPs) from the evolutionary synthesis models of Bruzual & Charlot (2003). The models were computed with the MILES library (Vazdekis et al. 2010), following Padova's evolutionary tracks with the initial mass function of Chabrier (2003). An SSP consists of $N_\star = 150$ elements, spanning six metallicities, $Z = 0.005$, 0.02, 0.2, 0.4, 1 and 2.5 $Z_\odot$, and 25 stellar population ages in the range from 1 Myr to 18 Gyr.

In the template-subtracted spectra, we measured automatically different important attributes of the spectral emission lines, like their flux and full width at half maximum (FWHM). Other important features retrieved from the stellar population templates fitted by STARLIGHT are the stellar velocity dispersions and the star formation history (SFH) of the host galaxies. The SFH map shows how the smoothed star formation rate (SFR) in a galaxy varies over a time period covering $\log(t) = 5.7$ yr to $\log(t) = 10.6$ yr (Asari et al. 2007).

2.1. *Morphologies and star formation history*

To determine the morphologies of the galaxies we used a composite method combining an eye estimate with the SFH. First, two of us (IP-F and RC) determined by eye the morphologies of the 409 isolated NELGs following the standard Hubble classification. Then, using only the galaxies with concordant morphologies–meaning the two observers gave exactly the same morphology–an average SFH prototype for each morphology class was created. Using these prototypes, the residuals of the SFH for each galaxy were calculated separately in three distinct time periods: Recent, $5.7 \leq \log(t/\mathrm{yr}) \leq 7.9$, Intermediate, $7.9 < \log(t/\mathrm{yr}) \leq 9.0$, and Old, $9.0 < \log(t/\mathrm{yr}) \leq 10.6$. A correction was then made to the eye morphology classification by choosing a morphology that minimized the variance of the residuals in each time period. For example, by eye we could have given the type S0 or Sa to a galaxy, but the residuals being minimal for Sa we adopted this last classification.

Once the morphologies were correctly adjusted to the SFH, we recalculated the prototypes by calculating the mean SFH in each morphological bin. Since we found the Sb and Sbc types to have SFH prototypes that are extremely similar and almost impossible to distinguish, we merged these two morphological bins together, keeping only the Sb identifi-

TABLE 1

EXAMPLES OF SPECTROSCOPIC CHARACTERISTICS OF THE ISOLATED NELGS[†]

Identification in SDSS	$\log\left(\frac{\mathrm{O[III]}}{\mathrm{H}\beta}\right)$	$\log\left(\frac{\mathrm{N[II]}}{\mathrm{H}\alpha}\right)$	Activity Type	$L_{\mathrm{H}\alpha}$ $L_{\odot}$	$\sigma_{\star}$ km s^{-1}	$\log(\lambda\ L_{5100})$ erg s^{-1}
SDSS J105809.84−004628.8	−0.364	−0.351	SFG	6.19	87	42.13
SDSS J113903.33−001221.6	0.228	0.060	AGN	6.05	144	42.56
SDSS J135807.05−002332.9	−0.604	−0.521	SFG	7.03	86	42.76
SDSS J142223.76−002315.5	−0.437	−0.494	SFG	5.50	81	41.16
SDSS J150654.85+001110.8	0.253	0.055	AGN	6.67	202	43.11
SDSS J113423.32−023145.5	0.363	0.238	AGN	6.23	136	43.00
SDSS J115425.04−021910.3	−0.275	−0.453	SFG	5.36	78	41.29
SDSS J122353.98−032634.4	−0.218	−0.148	TO	5.39	113	41.64
SDSS J124428.12−030018.8	−0.193	−0.300	TO	6.28	115	42.69
SDSS J170128.21+634128.0	−0.671	−0.375	SFG	7.20	99	42.52

[†]Full table available in electronic form at `http://www.astroscu.unam.mx/rmaa/RMxAA..47-2/RMxAA..47-2_rcoziol-tables.zip/`.

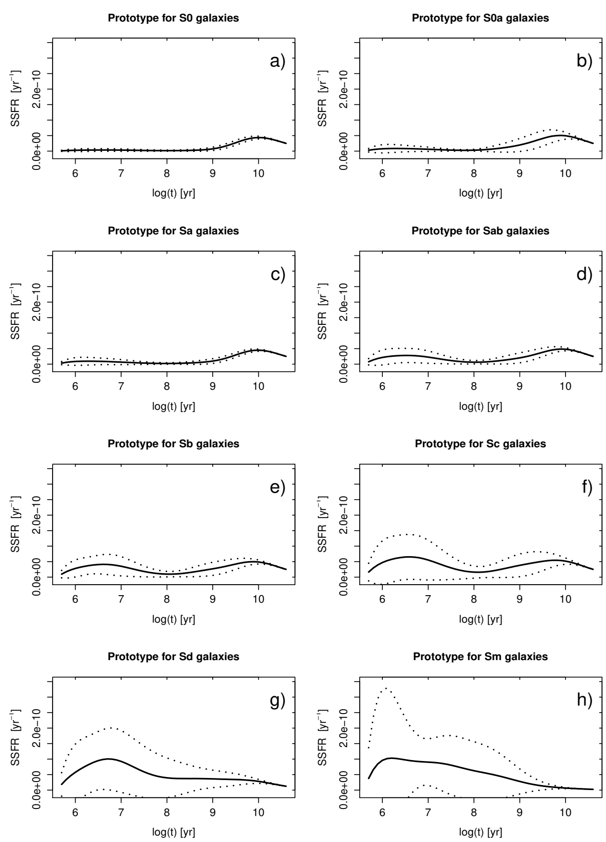

Fig. 2. SFH for the isolated NELGs. In each graph we show the mean prototype (solid line) and its dispersion at two sigma (dotted line). In order to use the same scale for all morphological classes, we have applied a factor of 0.5 and 0.1 to the SFH curves of the Sd and Sm, respectively.

cation. The final prototypes, including 327 (80%) of the 409 isolated NELGs, are presented in Figure 2. The prototypes suggest that S0, S0a, and Sa galaxies formed most of their stars in the past, $\log(t) > 9.0$ yr, while the Sab had a near constant star formation activity over the whole time lapse covered by STARLIGHT. This is also true for the Sb galaxies, but with a slightly larger dispersion. In the Sc galaxies, recent star formation activity becomes more important than in the past, but the dispersion also increases significantly the later the type. In Sd and Sm galaxies most of the stars appear to have formed recently, $\log(t) < 8.0$ yr. These results are in good agreement with similar studies based on integrated spectroscopy (e.g., Kennicutt 1992).

The remaining 20% galaxies were considered peculiar. Among these galaxies we count 36 late-type spirals (Sc or Sd) with a SFH typical of an Sa. These galaxies turned out to be cases where the fiber was covering only the innermost part of the galaxies. Also considered peculiar were 22 galaxies with a burst of star formation ∼100 Myr in the past. No external cause for the bursts could be determined, the galaxies being confirmed as isolated. Another 24 E or S0 galaxies were found to show a trace (not intense) of very recent star formation. All these peculiar galaxies were excluded from our analysis.

2.2. *Activity classification*

For our spectral activity analysis we further reduced our sample to 292 NELGs with a $\mathrm{S/N} \geq 3$ in the four most important emission lines: Hβ, [OIII]λ5007, Hα and [NII]λ6584. In Table 1 we com-

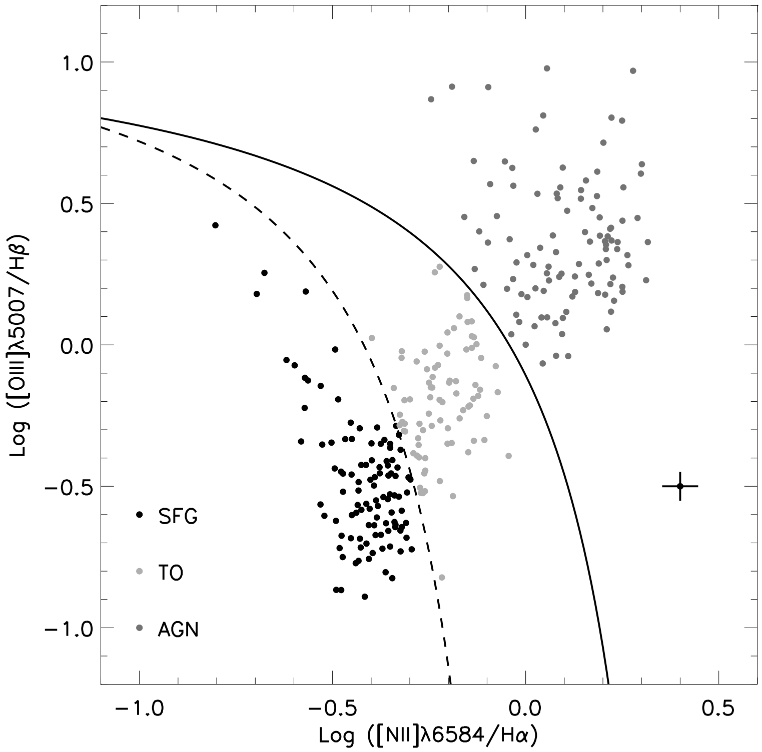

Fig. 3. Diagnostic diagram for the activity classification of the isolated NELGs. The separation between SFGs and TOs was suggested by Kauffmann et al. (2003) and the separation between TOs and AGNs by Kewley et al. (2006). Mean uncertainties on the line ratios are indicated as a cross on the lower right of diagram (not a datum). The color figure can be viewed online.

pile the spectroscopic characteristics of these galaxies as measured in the template subtracted spectra. Column 1 gives the SDSS identification of the galaxies. In Columns 2 and 3 we list the values of the two line ratios used to determine the activity type of the galaxies. The adopted classification is given in Column 4. In Column 5 we list the Hα emission line luminosity. In Column 6 we give the velocity dispersion of the stars, $\sigma_\star$, as deduced from the STARLIGHT template and corrected for the SDSS spectral resolution. Considering the size of the fiber used in SDSS ($3''$), this value can be taken as the stellar velocity dispersion of the bulge of the galaxy. Finally, in Column 7, we give the luminosity of the continuum at $\lambda5100$ Å as measured in the spectra before template subtraction.

We have identified the activity type of the 292 isolated NELGs in Figure 3, where we compare the two line ratios [OIII]$\lambda5007$/Hβ and [NII]$\lambda6584$/Hα. The typical low uncertainty levels on these ratios (cross in Figure 3) have practically no effect on our classification. We distinguish 105 SFGs (36.0%), 83 TOs (28.4%), and 104 AGNs (35.6%).

2.3. *Physical characteristics of the isolated NELGS*

We present the basic physical properties of the 292 isolated NELGs in Table 2. After the SDSS identification in Column 1, we list in Columns 2, 3 and 4 the right ascension, declination and redshift of the galaxies as listed in SDSS DR7. The results of our morphological classification are given in Column 5. Also from the SDSS DR7 database, we give in Columns 6 and 7 the Petrosian radii (in kpc) at 90% of the light distribution and the concentration index, CI, which is the ratio of the two Petrosian radii (CI $= R_{90\%}/R_{50\%}$). In Column 8 we list the luminosity in the K band as determined from 2MASS (K20 from 2MASS). In Column 9, we give the mean stellar age of the stellar populations consistent with the STARLIGHT template (Asari et al. 2007).

The K20 magnitudes from 2MASS were extracted from the extended sources catalog (Jarrett et al. 2000) by choosing the closest galaxy within 5 arcsecs of the best match. They were corrected for Galactic extinction at the position of the galaxies using the dust maps published in Schlegel et al. (1998). We also applied a k-correction using the method de-

TABLE 2

EXAMPLES OF BASIC PHYSICAL PROPERTIES OF THE ISOLATED NELGS

Identification in SDSS	RA (J2000) (degree)	DEC (J2000) (degree)	z	Morph.	$R_{90\%}$ kpc	CI	$\log(L_K)$ $L_{\odot}$	Mean (t_*) yr
SDSS J105809.84−004628.8	164.54102	−0.77468	0.0215	Sc	6.5	2.18	10.43	8.79
SDSS J113903.33−001221.6	174.76388	−0.20600	0.0181	Sab	8.6	3.06	10.77	9.82
SDSS J135807.05−002332.9	209.52940	−0.39248	0.0296	Sc	9.8	2.11	10.80	8.61
SDSS J142223.76−002315.5	215.59903	−0.38766	0.0055	Sd	4.6	1.90	10.01	7.81
SDSS J150654.85+001110.8	226.72857	0.18634	0.0351	Sa	12.1	2.72	11.19	9.60
SDSS J113423.32−023145.5	173.59719	−2.52933	0.0395	Sb	13.9	2.09	11.06	9.79
SDSS J115425.04−021910.3	178.60434	−2.31955	0.0080	Sd	4.5	2.12	9.78	8.05
SDSS J122353.98−032634.4	185.97495	−3.44292	0.0068	Sab	5.5	2.79	10.58	8.92
SDSS J124428.12−030018.8	191.11718	−3.00525	0.0239	Sc	8.6	2.65	10.61	9.17
SDSS J170128.21+634128.0	255.36758	63.69112	0.0163	Sc	5.5	1.76	10.42	7.89

[†]Full table available in electronic form at `http://www.astroscu.unam.mx/rmaa/RMxAA..47-2/RMxAA..47-2_rcoziol-tables.zip/`.

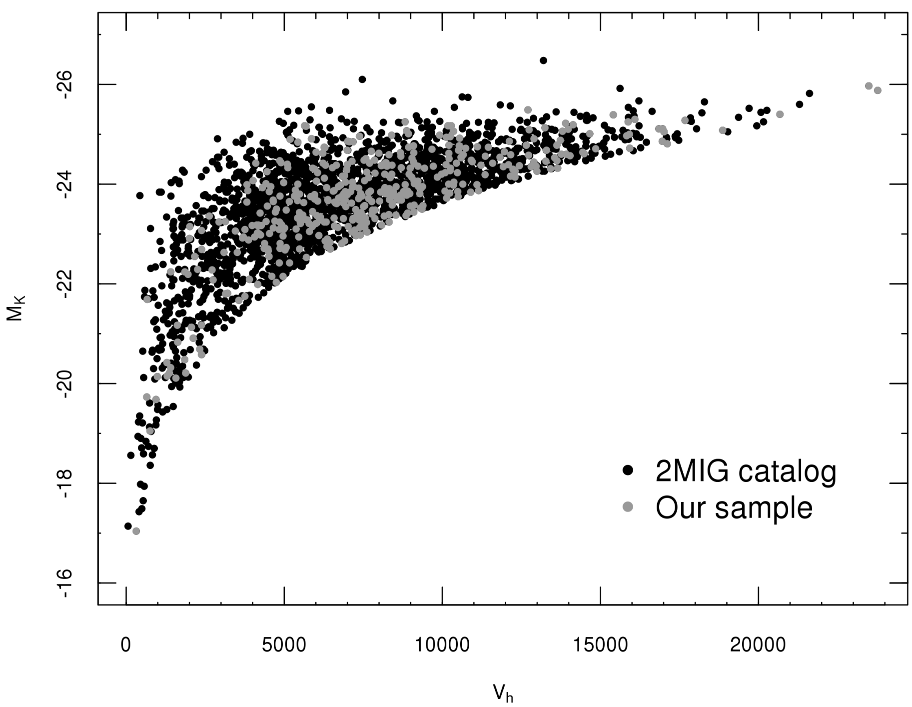

Fig. 4. Comparison of absolute K magnitude vs. heliocentric velocity for the 2MIG catalog and our subsample of 292 isolated NELGs. The color figure can be viewed online.

scribed in Kochanek et al. (2001). This method is reported to be valid for $z < 0.25$ and to be independent of the galaxy morphological type. The K band absolute magnitude was calculated using the standard relation:

$$M_K = m_K - 25 - 5\log(D_L) - A_K - k(z), \qquad (1)$$

where m_K is the total apparent magnitude in K, A_K is the Galactic extinction, D_L is the luminosity distance in Mpc, calculated assuming $H_0 = 75$ km s^{-1} Mpc^{-1}, and $k(z) = -6.0\log(1+z)$ is the k-correction. From the magnitudes we deduce the K luminosities applying the relation:

$$\log(L_K/L_{\odot}) = 0.4(M_{\odot K} - M_K), \qquad (2)$$

TABLE 3

DISTRIBUTION OF MORPHOLOGIES OF 292 ISOLATED NELGS

Morphology type	Number	Fraction %
S0	9	3.1
S0a	4	1.4
Sa	55	18.8
Sab	68	23.3
Sb	83	28.4
Sc	53	18.2
Sd	17	5.8
Sm	3	1.0

TABLE 4

EXAMPLES OF MASSES OF ISOLATED NELGS†

Identification in SDSS	$\log(M)(M_\odot)$		
	$M_{\rm Bulge}$	$M_{\rm BH}$	M_B
SDSS J105809.84−004628.8	9.04		10.71
SDSS J113903.33−001221.6	9.40	6.41	10.55
SDSS J135807.05−002332.9	9.17		11.04
SDSS J142223.76−002315.5	8.39		10.17
SDSS J150654.85+001110.8	9.99	7.06	11.12
SDSS J113423.32−023145.5	9.69	6.74	11.22
SDSS J115425.04−021910.3	8.52		9.86
SDSS J122353.98−032634.4	8.77	5.70	10.28
SDSS J124428.12−030018.8	9.33	6.33	10.96
SDSS J170128.21+634128.0	9.03		10.77

†Full table available in electronic form at `http://www.astroscu.unam.mx/rmaa/RMxAA..47-2/RMxAA..47-2_rcoziol-tables.zip/`.

TABLE 5

MEDIAN MASSES AND CONCENTRATION INDICES

	$\log(M)(M_\odot)$			CI
	$M_{\rm Bulge}$	M_K	M_B	
AGN	9.64	10.90	10.92	2.41
TO	9.41	10.85	10.78	2.21
SFG	9.10	10.66	10.56	2.11
S0/S0a	9.73	10.98	10.94	3.21
Sa	9.72	10.91	11.00	2.87
Sab	9.46	10.82	10.78	2.62
Sb	9.39	10.94	10.77	2.34
Sc	9.10	10.66	10.58	2.12
Sd	8.44	9.86	9.66	2.07

where $M_{\odot K} = 3.28$ is the absolute magnitude of the Sun in the K band (Binney & Merrifield 1998). From the uncertainties in the fluxes (Jarrett et al. 2000), a mean uncertainty of 6% is estimated for our K luminosities.

In Figure 4 we compare the distributions of the 2MASS absolute magnitudes in K and heliocentric radial velocities, as found in our subsample of 292 isolated NELGs and in the entire 2MIG catalogue. The distribution for the 2MIG catalogue is typical of a flux limited survey. The galaxies of our subsample are randomly distributed, suggesting they form a statistically fair sample of all the isolated galaxies in the 2MIG catalogue.

3. ANALYSIS

3.1. *Activity type vs. morphology*

We present the fractions of morphology types in our sample of 292 isolated NELGs in Table 3. The majority (70.5%) of these galaxies are classified as intermediate spirals (Sa-Sab-Sb). In Figure 5 we show how the distribution of activity type varies in the different morphology classes: AGNs and TOs are mostly found in early-type galaxies (S0-Sa), while the proportion of SFGs gradually increases in later types (Sab-Sm). This result is not new, but confirms the common view about AGNs in the field: they are mostly found in early-type spiral galaxies (e.g., Melnick, Terlevich, & Moles 1986; Osterbrock 1989; Blandford, Netzer, & Woltjer 1990).

In Table 4 we give our estimated masses for the bulges, $M_{\rm Bulge}$, as determined using the velocity dispersions, $\sigma_\star$, and applying the virial theorem. The box-whisker plots for the bulge masses of the galaxies separated by activity type are presented in Figure 6a. The median values are reported in Table 5. AGNs and TOs possess more massive bulges than SFGs. The trends observed for the AGNs and TOs are confirmed using a non-parametric statistical test (Kruskall-Wallis with Dunn's multiple comparison tests). The results of these tests are presented in Table A1 of the Appendix. The tests find the medians in the three samples to be significantly different at a level of confidence of 99%.

In Figure 6b we compare the bulge mass of galaxies with different morphologies. We also observe a significant difference, the bulge mass being larger in

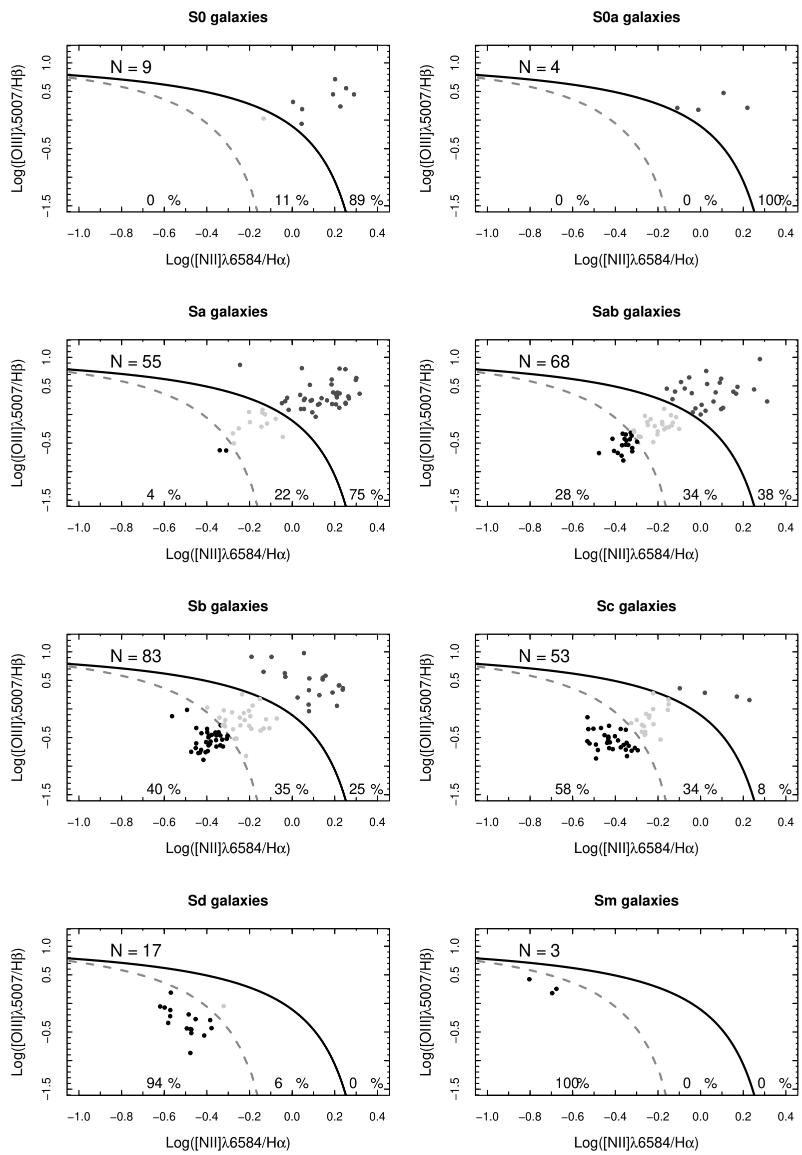

Fig. 5. Diagnostic diagrams for isolated NELGs with different morphologies. The separations and colors are as explained in Figure 3. The color figure can be viewed online.

earlier morphological types. This trend is also found to be statistically significant. The results for the tests, presented in Table A2 of the Appendix, show that the farther apart the morphological class, the more significant the difference in bulge mass. For example, the statistical tests reveal no difference between Sa and Sab, but a significant one between Sa and Sb. Similarly, no difference appears between Sab and Sb, but a significant one is found between Sab and Sc.

The above results lead to the question of whether the most important parameter is the mass of the bulge or the morphology of the galaxy. As a test, we compare the bulge masses in two statistical groups: Group 1 which is composed of Sa and Sab galaxies, and Group 2 which is composed of Sab and Sb. The box-whisker plots are drawn in Figure 7a for Group 1 and Figure 7b for Group 2. We find no significant difference in bulge mass between the different activity types in Group 1, while in Group 2 there is a significant difference only between the SFGs and AGNs. This is confirmed by the statistical tests in Table A1 of the Appendix. We conclude that the AGN activity is related to the bulge mass, but mostly because of the strong connection of this parameter with the morphology: the earlier the morphology, the larger

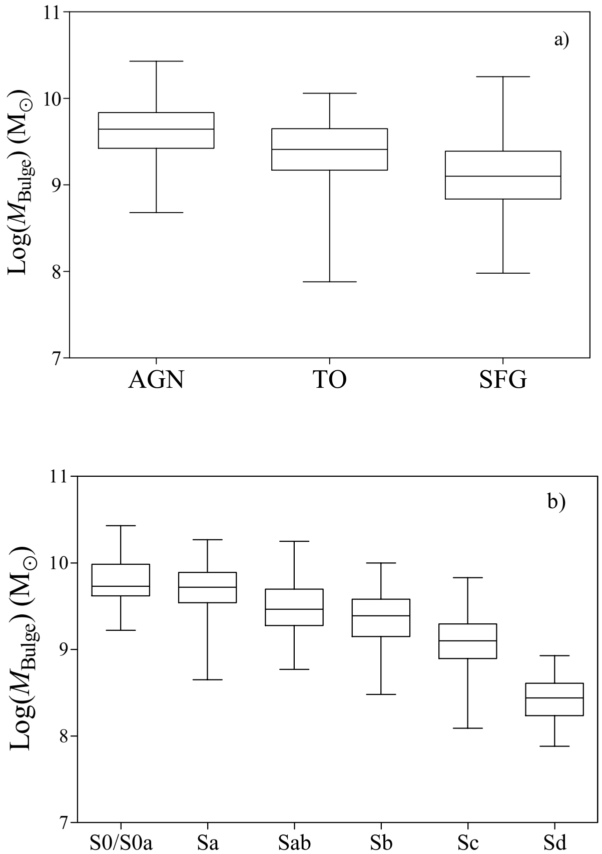

Fig. 6. Box-whisker plots for the bulge masses of galaxies as function of (a) activity type, (b) morphology. The middle line is the median, the box is limited by the percentiles and the whiskers indicate the full range of values.

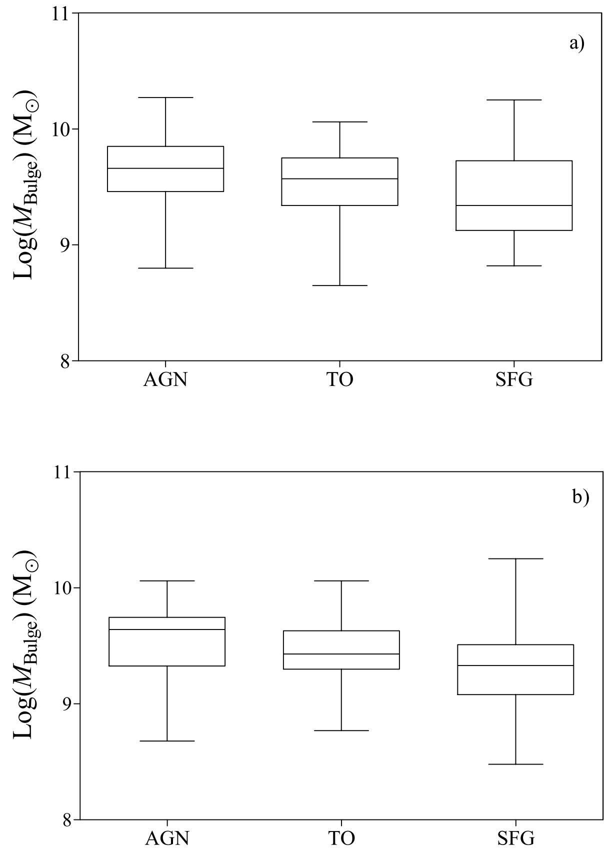

Fig. 7. Box-whisker plots for the bulge masses as found (a) in group 1 (Sa and Sab galaxies), and (b) in group 2 (Sab and Sb galaxies). Box-whiskers are defined as in Figure 6.

the bulge mass, and the higher the probability to see an AGN. This is also consistent with the diagnostic diagrams, which show a larger frequency of AGNs in earlier morphological types. In Group 1, the numbers of AGNs, SFGs and TOs are 67, 21 and 35, respectively, while in Group 2 these numbers change to 47, 53 and 51 respectively. For an increase by a factor of 2 in bulge mass, from Sa to Sb (the bulge mass increases by factor of 3.5 from AGN to SFG in Table 5), the number of AGNs slightly falls and the number of TOs and SFGs doubles.

The bulge mass being an important morphological parameter, the strong correlation found with AGN activity suggests this phenomenon is intimately connected with the formation process of the galaxies.

3.2. *Activity type vs. galaxy mass*

We have estimated the masses of our galaxies using two different methods. The first method is based on 2MASS K band luminosities (as compiled in Table 2), while the second is based on the absolute B magnitudes, which were obtained using the Johnson-B band magnitude synthesized from the SDSS magnitudes (Fukugita et al. 1996). The absolute magnitudes in B are compiled in Tables 6, 8 and 9, for the SFGs, AGNs, and TOs, respectively. The uncertainty is of the order of 0.05 mag. Being insensitive to dust extinction and to the morphological type of the galaxies the near-infrared emission is a better tracer of the stellar mass than the B magnitudes, for which we need to apply a correction depending on the morphology.

The K luminosities were transformed into masses using the mass-to-light ratio $M/L_K = 0.95$, as estimated by Bell et al. (2003). To transform the B absolute magnitudes into masses, we first corrected for galactic extinction and k-correction using the code developed by Blanton & Roweis (2007). Then we applied the different mass-to-light ratios for galaxies

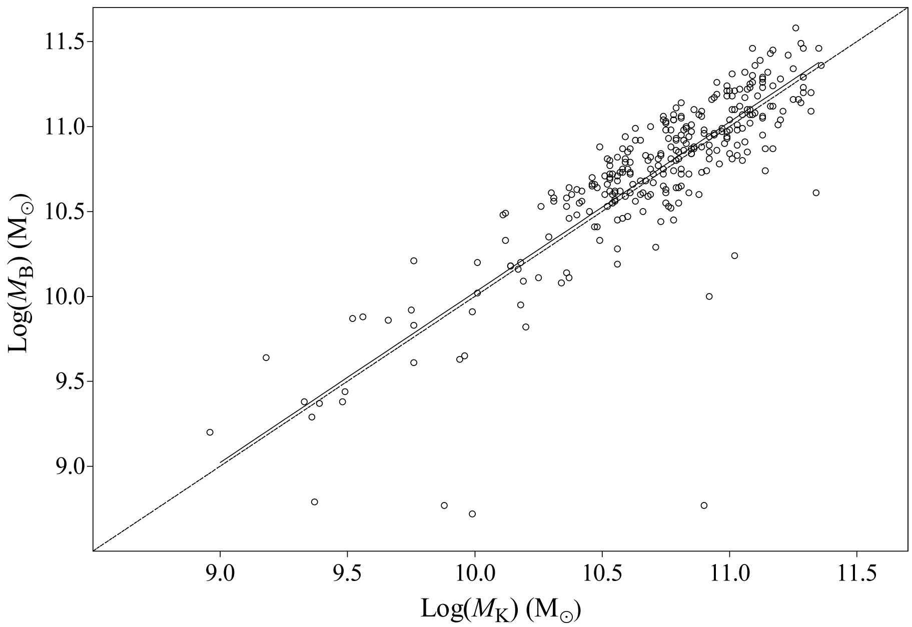

Fig. 8. Comparison of the two mass estimates. The dotted line is the one-to-one relation and the continuous line is a linear fit.

as published by Faber & Gallagher (1979). These ratios were adjusted for our adopted value of the Hubble constant. The B mass estimates appear in Column 4 of Table 4.

In Figure 8 we compare the two mass estimates. The linear relation fitted has a correlation parameter $r^2 = 0.72$, implying that 72% of the total variance of the B mass estimates is explained by the variation of the K mass estimates (and vice versa). The median values for the masses in the B and K bands are given in Table 5. They are in excellent agreement with those reported by Roberts & Haynes (1994) for galaxies having similar morphological types.

In Table 5 we see that both median masses, M_B and M_K, tend to increase from the SFGs to the AGNs. The general trend observed in the box-whisker plots presented in Figure 9 looks slightly more obvious using M_K than M_B. In Table A1 of the Appendix we see that using M_B the statistical tests detect a slightly more significant difference between the AGNs and SFGs than between the TOs and SFGs, while both differences are similarly statistically significant using M_K. No significant difference is observed between the AGNs and TOs.

In Figure 10 we compare the masses of the galaxies having different morphological types. Although we found a significant variation of the bulge mass with the morphology, the total mass M_B and M_K do not seem to vary as much between galaxies having different morphologies. In Table A2 of the Appendix, we find that the observed differences start to be statistically significant only when the comparison is done with the latest types, Sc for M_B, and even later, Sd, for M_K. We conclude that galaxies with different morphologies show only marginal differences in their total masses.

Based on our analysis, the trends observed between the AGN activity, the bulge mass and morphology does not appear to be "quantitative" (based on a difference in total mass), but more "qualitative", the AGN activity appearing more frequently when a higher fraction of the mass of the galaxy is in the form of a bulge. This seems to favor a mechanism based on different astration rates–defined as the efficiency with which a galaxy transforms its gas into stars (Sandage 1986). The higher the astration rate, the more massive the bulge and the higher the probability to observe an AGN.

3.3. *Relation with stellar populations*

In Figure 11 we compare the distributions of the mean ages of the stellar populations in galaxies showing different activity types. The stellar populations of the SFGs are dominated by young stars, with mean ages ranging from 0.32 to 1.0 Gyr. These values correspond to the 25 and 75 percentiles, respectively. The mean age of the stellar populations is observed to go up in the TOs, with values ranging

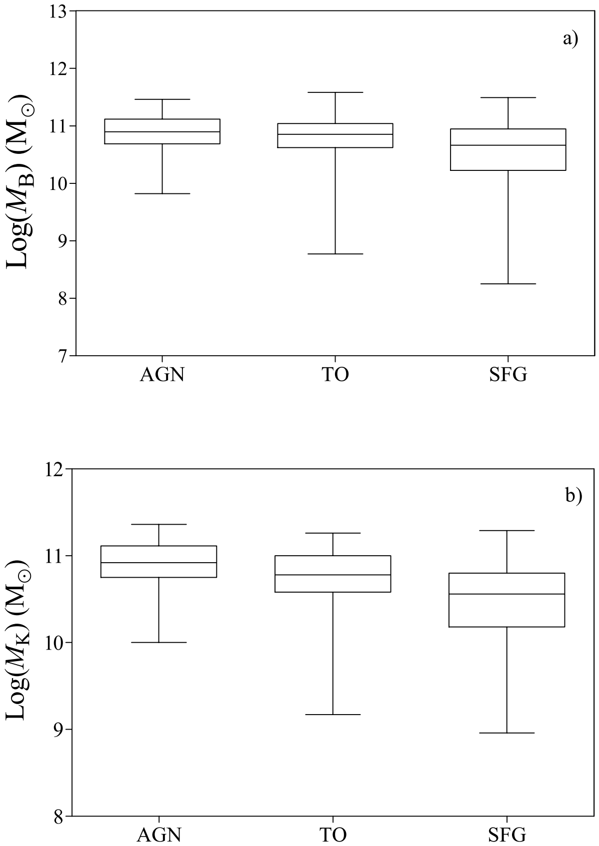

Fig. 9. Box-whisker plots for the total masses in galaxies showing different activity types; (a) M_B and (b) M_K.

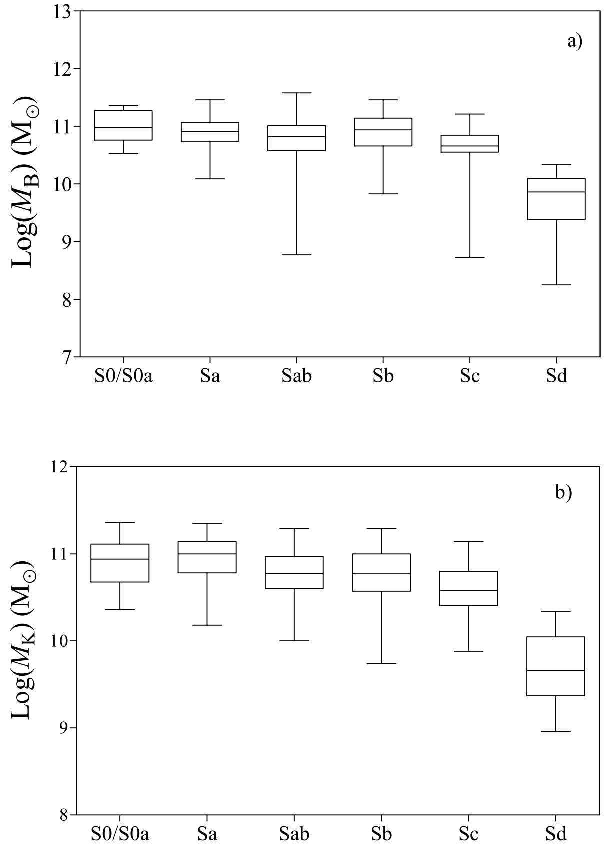

Fig. 10. Box-whisker plots for the total masses in galaxies having different morphologies; (a) M_B and (b) M_K.

from 0.5 to 3.2 Gyr, and to culminate in the AGNs with values ranging from 1.6 to 6.3 Gyr. Comparable results were encountered before by Boisson et al. (2000).

A strong connection is also found with the morphologies. In Figure 12 the morphologies were regrouped into three broad classes: Late (Sc, Sd, and Sm), Intermediate (Sa, Sab, and Sb), and Early (S0 and S0a). The SFGs show a mixture of Late and Intermediate morphologies, while the TOs have only Intermediate morphologies. The AGNs on the other hand have mostly Early morphologies.

The correlations between morphology, activity type and mean stellar ages of the stellar populations support a strong connection between the AGN activity and the formation process of the galaxies. In particular, the AGN phenomenon appears like a normal by-product of the formation process of galaxies that produces more massive bulges.

There are many structural similarities between the bulges of spiral galaxies and elliptical galaxies, suggesting similar formation mechanisms (e.g.,

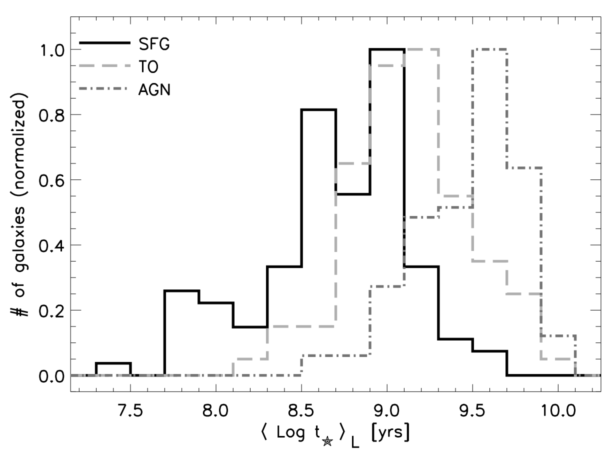

Fig. 11. Distributions of mean ages of stellar populations for galaxies with different activity types. The color figure can be viewed online.

Jablonka, Martin, & Arimoto 1996). In particular, elliptical galaxies are known to have endured higher astration rates than spiral galaxies when they formed

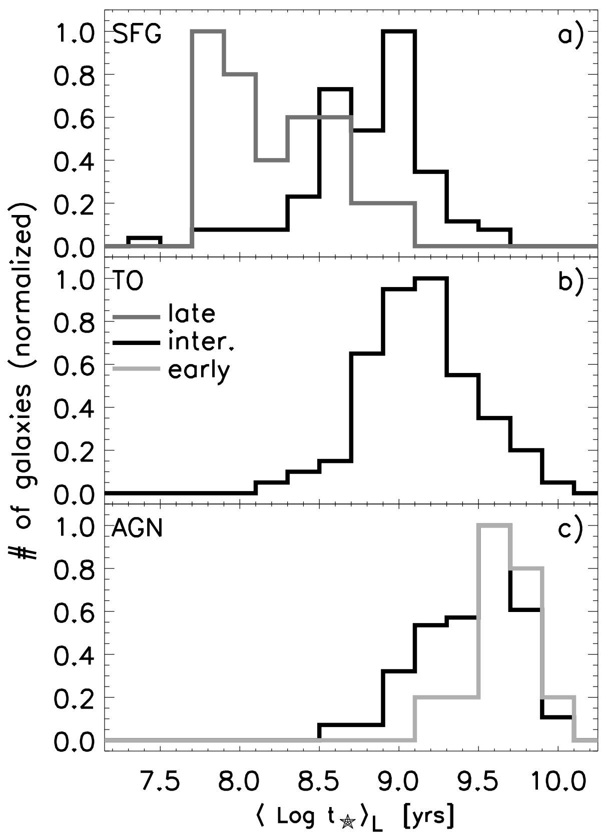

Fig. 12. Distributions of mean ages of stellar populations for galaxies with different activity types and different morphologies. The color figure can be viewed online.

(Sandage 1986), transforming almost all their gas into stars in a very short period of time. Assuming that galaxies form by a succession of star forming episodes–an assumption necessary to produce the mass-metallicity relation–galaxies with high astration rates would thus be expected to have formed most of their stars in the past because, the reservoir of gas being limited, the galaxy would have consumed it rapidly and stopped forming stars relatively early. This would explain the differences in mean ages for the stellar populations observed in our sample of isolated NELGs.

3.4. *Relation with gas metallicity*

After correcting for dust absorption, the metallicities of the gas in the SFGs were estimated using the empirical correlation found between log(O/H) and the emission-line ratio R_3 = ([OIII]λ4959 + [OIII]λ5007)/Hβ (Edmunds & Pagel 1984; Vacca & Conti 1992). The correlation originates from the cooling effect of oxygen: as the metallicity of the gas increases, the gas is cooled more efficiently, the

TABLE 6

EXAMPLES OF GAS METALLICITIES AND ABSOLUTE B MAGNITUDES OF SFGS[†]

Identification in SDSS	[O/H]	M_B
SDSS J105809.84−004628.8	0.26	−18.46
SDSS J135807.05−002332.9	0.43	−19.68
SDSS J142223.76−002315.5	0.31	−17.11
SDSS J115425.04−021910.3	0.20	−16.35
SDSS J170128.21+634128.0	0.47	−18.65
SDSS J214907.29+002650.3	0.51	−18.28
SDSS J235106.25+010324.1	0.48	−17.67
SDSS J021859.64+001948.0	0.44	−18.69
SDSS J025154.58+003953.3	0.29	−19.06
SDSS J003823.71+150222.4	0.38	−18.69

[†]Full table available in electronic form at `http://www.astroscu.unam.mx/rmaa/RMxAA..47-2/RMxAA..47-2_rcoziol-tables.zip/`.

temperature drops and the line ratio R_3 decreases (McCall, Rybski, & Shields 1985; Evans & Dopita 1985).

The gas metallicities in the SFGs are compiled in Table 6, together with their absolute B magnitudes. We assume the solar metallicity is $12 + \log(\mathrm{O/H}) = 8.66 \pm 0.05$ (Asplund et al. 2004). The uncertainty in the metallicities is of the order of ± 0.2 dex (Edmunds & Pagel 1984). In Figure 13 we plot the gas metallicities in the SFGs against their absolute B magnitudes. The results are in excellent agreement with what is expected based on their late-type morphologies (Zaritsky, Kennicutt, & Huchra 1994). The results are also in good agreement with what was observed in Starburst Nucleus Galaxies (SBNGs): the gas in the late-type SBNGs is more metal rich than in the early-type SBNGs, due to their different formation processes (Coziol et al. 1998b).

The usual way to determine the metallicity of AGNs is to compare the observed line ratios with the outputs obtained using an ionization code like CLOUDY (Ferland et al. 1998). However, the results are usually ambiguous, with more than one possible solution (Nagao, Maiolino, & Marconi 2006). There maybe also other physical mechanisms, like shocks or special ionizing structures, that can complicate the interpretation based solely on photoionization model results (Viegas & de Gouveia dal Pino 1992; Cooke et al. 2000).

An excellent study was presented recently by Bennert et al. (2006). With the permission of the

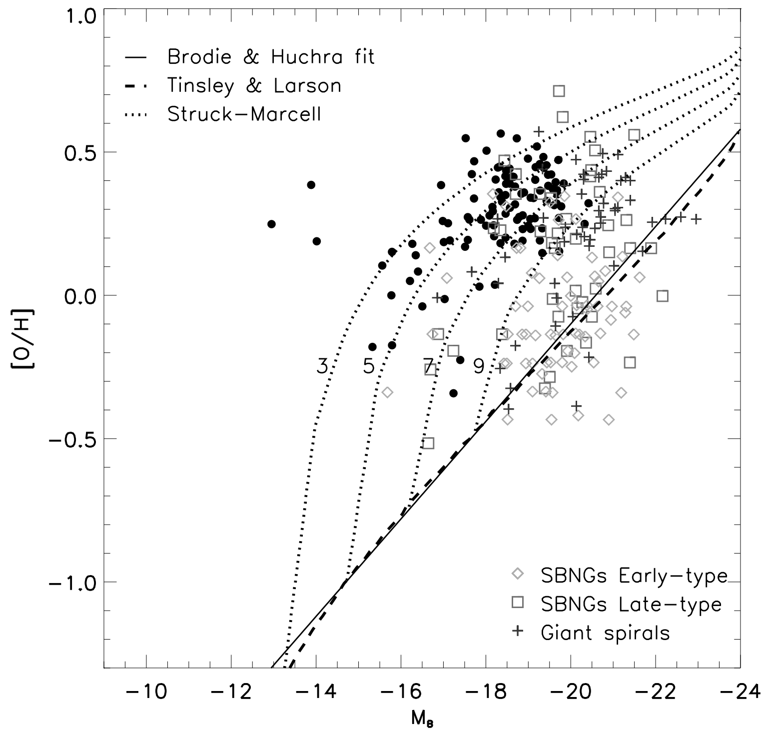

Fig. 13. Gas metallicities vs. absolute B magnitudes for the SFGs (filled dots). The giant spirals sample is taken from Zaritsky et al. (1994) and the SBNGs from (Coziol et al. 1998b). The continuous straight line is the Brodie-Huchra (1991) relation for elliptical galaxies. Also shown are two models of multiple mergers by Tinsley & Larson (1979) and Struck-Marcell (1981). The numbers indicate the approximate number of mergers necessary in the models to reproduce the metallicities. The color figure can be viewed online.

authors, we reproduce some of their results in Figure 14. The models discussed in their study apply exactly to our NELGs. From their study we can see that the line ratio [NII]/Hα is extremely sensitive to the abundance of nitrogen. One possible cause for the increase of nitrogen emission in the AGNs could be an excess of nitrogen (Osterbrock 1970; Storchi-Bergmann & Pastoriza 1989; Storchi-Bergmann 1991; Hamann & Ferland 1993). In the center of galaxies with massive bulges and old stellar populations, we do not expect the nitrogen abundance to follow the normal secondary relation (Zaritsky et al. 1994; Thurston, Edmunds, & Henry 1996; van Zee et al. 1998; Coziol et al. 1999).

In Figure 14 we also observe that, for any value in excess of nitrogen abundance, increasing the ionizing parameter, U, while keeping the metallicity constant causes the ratio [OIII]/Hβ to rise. But, if we increase U too much the ratio [NII]/Hα begins to decrease. In the same figure we observe that when we lower the metallicity while keeping U constant, both line ratios increase, which is consistent with the cooling effect of oxygen. However, if we decrease the metallicity too much, both line ratios eventually decrease. This behavior is consistent with a coupling effect between U and the metallicity (Evans & Dopita 1985): as the metallicity decreases, U increases and vice versa. Therefore, one can arbitrarily change one parameter or the other with almost the same effect.

In Figure 14 the TOs and AGNs trace a continuous sequence where the ratios [NII]/Hα and [OIII]/Hβ increase together. According to the CLOUDY models of Bennert et al. one way to explain this sequence would be to decrease the metallicity gradually while increasing the overabundance of nitrogen. Consistent with this model, we fitted on the TOs and AGNs distributions an empirical relation between the ratio [OIII]/Hβ and [NII]/Hα. We then searched for a calibration that would yield the same range in metallicities for the TOs as obtained using the model of Bennert et al. (2006), from 2.5 to 1 $Z_\odot$. As a first approximation we found that the R_3 calibration for the SFGs nearly reproduces these values. Extrapolating this calibration over the AGNs region suggests a decrease in metallicities for these objects from 1 $Z_\odot$ to 0.3 $Z_\odot$. Based on the models of

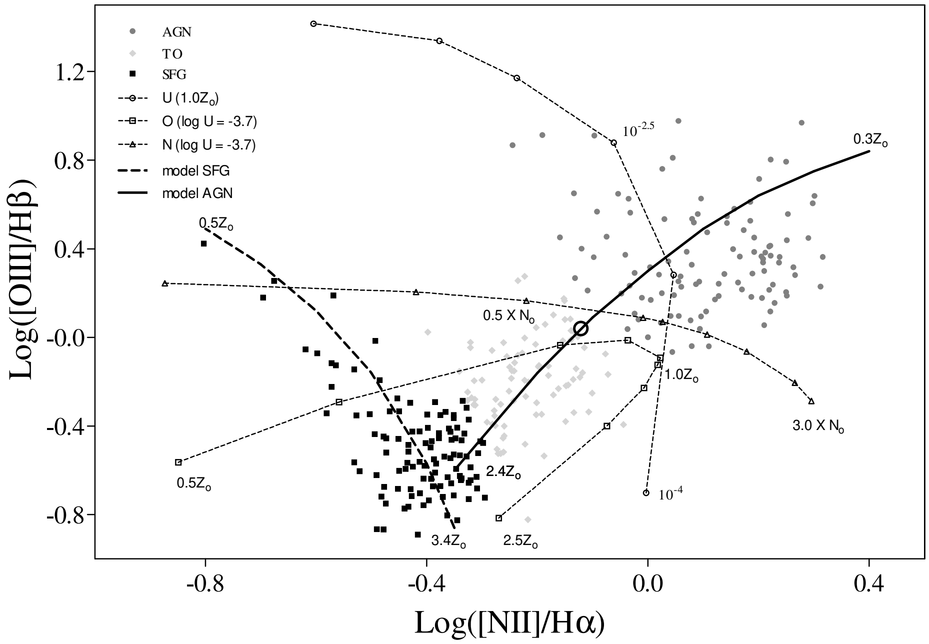

Fig. 14. Diagnostic diagram with three curves obtained by Bennert et al. (2006) using CLOUDY: U, varying the ionizing parameter at constant solar metallicity; O, varying the metallicity keeping U constant; N, varying the nitrogen abundance. Also shown is our calibration using R_3. The bold circle on this curve corresponds to 1.0 $Z_\odot$. The color figure can be viewed online.

Bennert et al. (2006), the ionizing parameter would increase from $10^{-3.5}$ to $10^{-2.5}$, which seems in good agreement with the values found by Baskin & Laor (2005), and the abundance of nitrogen would not exceed 2 times the solar value, which is a lower excess than suggested originally by Osterbrock (1970), but still fully consistent with what is observed in the bulges of normal galaxies (Thurston et al. 1996; van Zee et al. 1998; Coziol et al. 1999).

Our model suggests that there is an inversion in the metallicity-nitrogen abundance relation in the AGNs compared to that in the SFGs: in the SFGs, the nitrogen abundance increases with the metallicity, while in the TOs and AGNs the nitrogen abundance increases as the metallicity decreases (consistent with an excess in nitrogen abundance). For the TOs and AGNs the relation is:

$$[\mathrm{O/H}] = -0.52 + (\log([\mathrm{NII}]/\mathrm{H}\alpha) - 0.6)^2\,. \quad (3)$$

For the SFGs the relation is:

$$[\mathrm{O/H}] = -[0.99 + 0.61/(\log([\mathrm{NII}]/\mathrm{H}\alpha) - 0.05)]\,. \quad (4)$$

To test our calibration, we searched the literature for NLAGNs for which the metallicity of the gas was previously estimated using CLOUDY, and could also be evaluated by our method (with reported spectrophotometry in the optical). We found very few examples, and all are Sy2 located in the upper part of our diagram in Figure 15, where we expect our calibration to yield the most discrepant results. The values obtained are compiled in Table 7.

TABLE 7

GAS METALLICITIES OF AGNS FROM THE LITERATURE, COMPARED TO THOSE OBTAINED USING OUR CALIBRATION

ID	$Z/Z_\odot$ (lit.)	$Z/Z_\odot$ (ours)	Literature sources
Mrk 78	0.30	0.30	(1)(2)
NGC 3393	0.10	0.21	(3)
NGC 1068	0.30	0.16	(4)
NGC 4507	0.50	0.27	(4)
NGC 5135	0.2-0.5	0.43	(4)
NGC 5506	0.50	0.23	(4)
Mrk 1388	0.70	0.23	(4)

(1)Ramos Almeida et al. 2006, (2) Ulrich 1971, (3) Cooke et al. 2000, (4) Nagao et al. 2006.

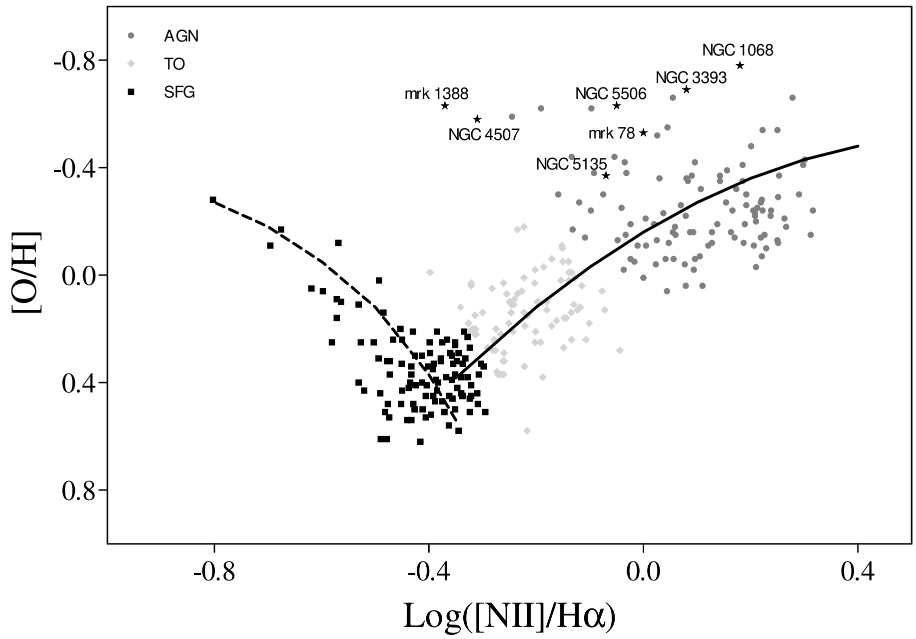

Fig. 15. Metallicity calibrated diagnostic diagram. The two empirical relations (equations 3 and 4) are also traced over the data. Also shown are Sy2 galaxies from the literature for comparison. The color figure can be viewed online.

Only the low metallicity solutions reported by Nagao et al. (2006) for their objects are consistent with our model. Surprisingly, the differences observed are not systematic, suggesting that other physical parameters (e.g., shocks, as we mentioned before, or special geometries, like an ionization cone or an obscuring torus) could also be important in these galaxies.

The above comparison suggests that the uncertainty in our metallicities is of the order of 0.3 dex, increasing to as much as 0.5 dex in some Sy2 like Mrk 1388. However, this galaxy appears to be an extreme case, for which we do not expect our calibration to apply. In Figure 15, most of the AGNs and TOs in our sample fall in a different regime than the AGNs from the literature used for the test (that is, the AGN in our sample fall in a different part of the diagnostic diagram, and they are clearly tracing a continuous relation). A better estimate of the uncertainty in the gas metallicities obtained with our method may be ∼0.2 dex, which is consistent with the variance of our fitted relation.

The gas metallicities as deduced from our calibration together with the B luminosities are presented in Table 8 for the AGNs, and in Table 9 for the TOs. In Figure 16 we show the box-whisker plots for the gas metallicities in galaxies having different activity types and different morphologies. The AGNs and TOs have lower gas metallicities than the SFGs and we find an excellent correlation with the morphological type of the galaxies, the metallicities increasing in the later types. The statistical tests (Table A1 and Table A2 in the Appendix) confirm the differences observed at a level of confidence of 99%.

TABLE 8

EXAMPLES OF GAS METALLICITIES AND ABSOLUTE B MAGNITUDES OF AGNS[†]

Identification in SDSS	[O/H]	M_B
SDSS J113903.33−001221.6	−0.15	−18.06
SDSS J150654.85+001110.8	−0.16	−19.52
SDSS J113423.32−023145.5	−0.24	−19.75
SDSS J172613.73+620858.1	−0.19	−18.85
SDSS J173044.85+562107.1	−0.35	−19.25
SDSS J025017.75−083548.5	−0.20	−17.84
SDSS J032501.68−054444.8	−0.06	−18.25
SDSS J142757.71+625609.3	−0.22	−19.46
SDSS J114743.68+014934.3	−0.66	−19.12
SDSS J133548.24+025956.1	−0.36	−19.28

[†]Full table available in electronic form at `http://www.astroscu.unam.mx/rmaa/RMxAA..47-2/RMxAA..47-2_rcoziol-tables.zip/`.

In Figure 17 we compare the gas metallicities of the TOs and AGNs with those of the SFGs.

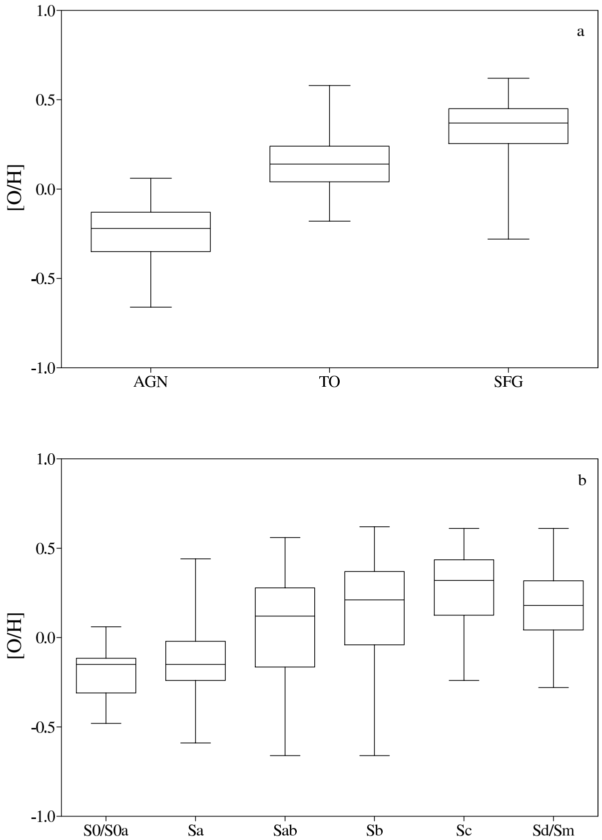

Fig. 16. Box-whisker plots for the gas metallicity variation in galaxies having (a) different activity types, and (b) different morphologies.

The AGNs seem to follow the Brodie-Huchra (1991) mass-metallicity relation for elliptical and bulge-dominated galaxies (Zaritsky et al. 1994; Coziol et al. 1998b). The TOs, on the other hand, with their intermediate morphologies, show also metallicities which are intermediate between those of the SFGs and the AGNs. The differences in metallicities observed between the SFGs, TOs and AGNs are in excellent agreement with the differences in mean ages of the stellar populations and bulge masses. All these parameters are consistent with higher astration rates for the AGNs as compared to the SFGs (Sandage 1986).

4. DISCUSSION

Our study suggests that the formation of a SMBH in the center of a galaxy is tightly connected with the formation process of its bulge (Häring & Rix 2004; Peterson et al. 2005; Gültekin et al. 2009). Some authors have even suggested that the formation of the bulge is a self-regulated process with strong feedback from the SMBH growing in its center (see Younger et al. 2008 and references therein). Our observations may support such interpretations.

TABLE 9

EXAMPLES OF GAS METALLICITIES AND ABSOLUTE B MAGNITUDES OF TOS[†]

Identification in SDSS	[O/H]	M_B
SDSS J122353.98−032634.4	0.16	−17.40
SDSS J124428.12−030018.8	0.14	−19.10
SDSS J224424.36−000943.5	0.24	−19.44
SDSS J020540.31−004141.4	0.21	−19.37
SDSS J031347.83+004139.7	0.10	−19.27
SDSS J032406.50−010328.2	0.03	−18.49
SDSS J012853.25+134737.6	0.02	−18.95
SDSS J030848.32−070226.1	0.28	−19.53
SDSS J033358.81−070826.6	0.10	−18.82
SDSS J090513.20−002947.8	−0.01	−17.82

[†]Full table available in electronic form at `http://www.astroscu.unam.mx/rmaa/RMxAA..47-2/RMxAA..47-2_rcoziol-tables.zip/`.

According to Aller & Richstone (2007) the gravitational binding energy is one key factor explaining the relation between the SMBH and the bulge mass. The gravitational binding energy is the negative of the gravitational potential energy. For a system of N particles, with an approximate mass $M = Nm_p$, where m_p is the mass of a proton, the binding energy per baryon is equal to:

$$U/N = GMm_p/R\,, \tag{5}$$

where G is the gravitational constant and R is the radius of the object. By definition, a SMBH represent a huge mass, which represents maybe only 1% to 0.1% of the bulge mass, but which is concentrated in an extremely small region of space at the center of mass of the galaxy. The formation of such a highly gravitationally bound object implies a significant increase in binding energy of the host galaxy itself.

The above description gives us a new test for the NLAGNs in our sample. If these galaxies host a SMBH in their center, we would expect them to show relatively high gravitational binding energies compared to, for example, the SFGs. To verify this assumption, we have used the masses as determined from the K magnitudes, M_K, and the Petrosian radii, $R_{90\%}$, reported in Table 2, to calculate the gravitational binding energy per baryon of all the galaxies in our sample. As expected, we observe in

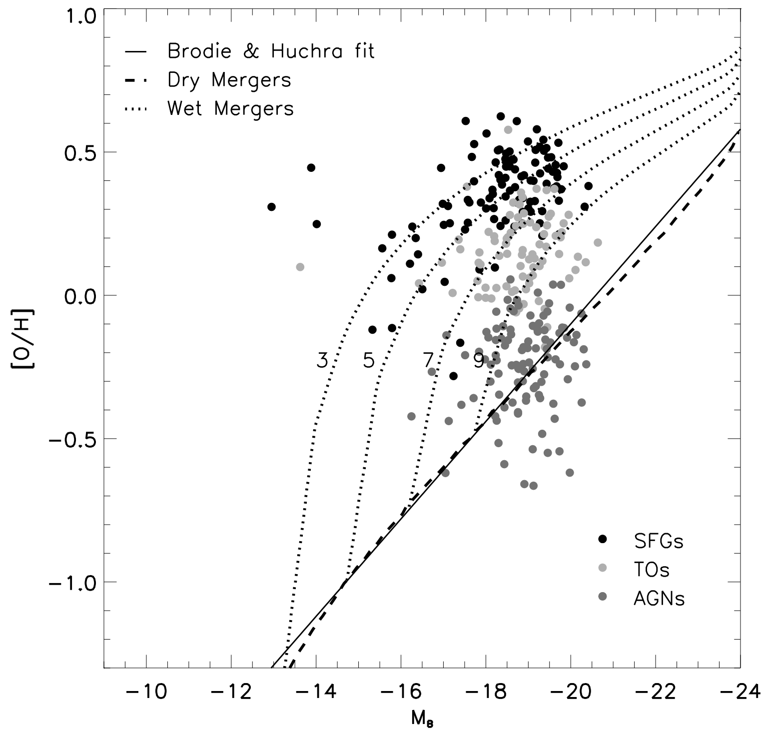

Fig. 17. Gas metallicities vs. absolute *B* magnitudes for all the isolated NELGs. The multiple merger model of Tinsley & Larson (1979) is identified as the dry merger scenario and the Struck-Marcell (1981) model is denoted as the wet merger scenario (see explanations in our discussion section). The color figure can be viewed online.

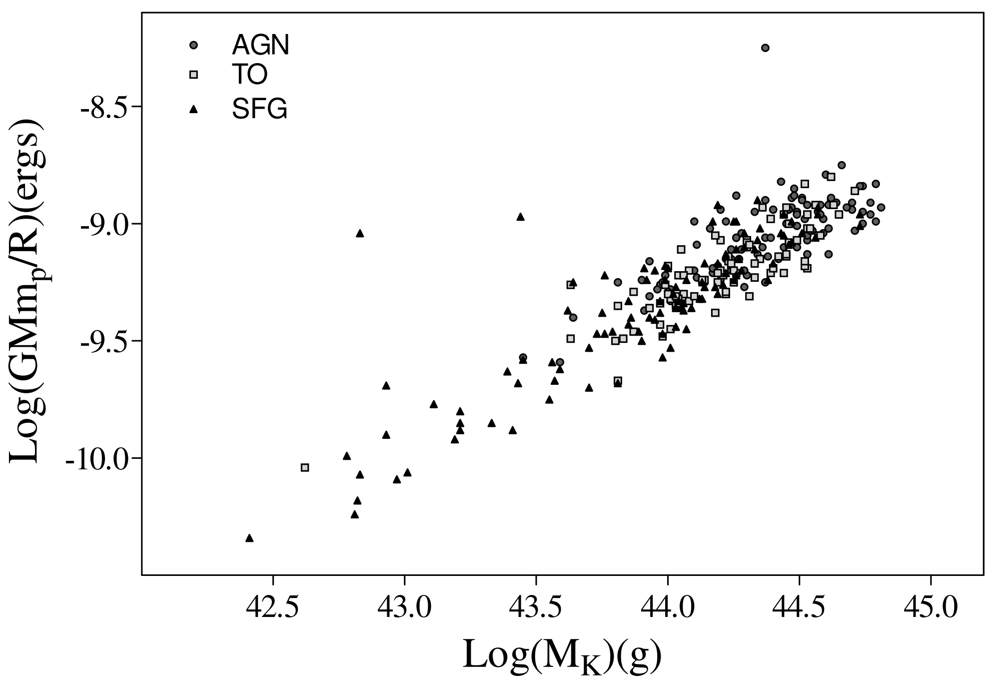

Fig. 18. Gravitational potential energy per baryon of the galaxies in our sample. The color figure can be viewed online.

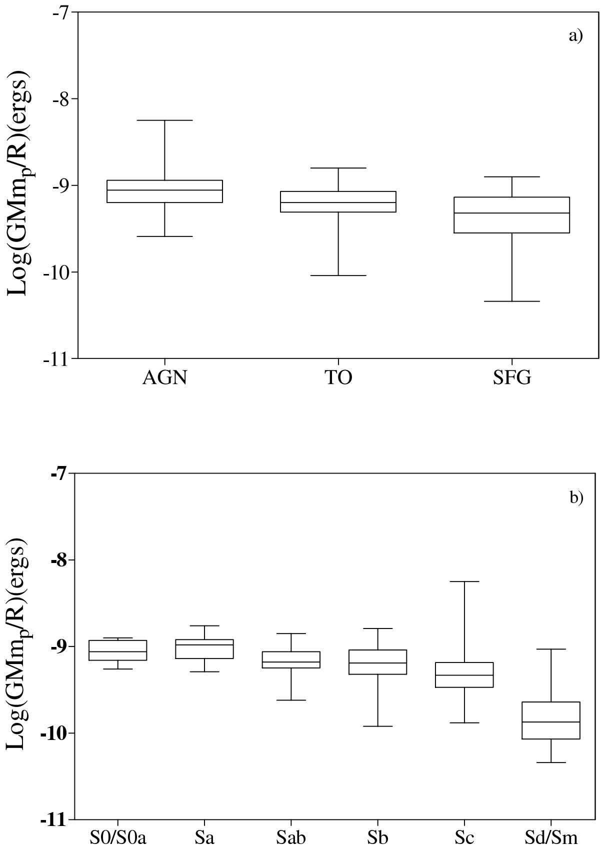

Fig. 19. Box-whisker plot of gravitational potential energy per baryon of the isolated NELGs, (a) with different activity types, (b) with different morphologies.

Figure 18 that the AGNs and TOs have higher gravitational binding energies than the SFGs. This trend is better seen in Figure 19a, which shows the box-whisker plots for the gravitational binding energies. The trend is also confirmed to be statistically significant in Table A1 of the Appendix.

The variation of gravitational binding energies with galaxy morphologies is shown in Figure 19b, and the trend is statistically tested in Table A2 of the Appendix. Galaxies with massive bulges, S0, S0a, and Sa, have comparable gravitational binding energies, which are significantly higher than those of galaxies having less massive bulges, Sab and later. These results are in good agreement with the hypothesis of a SMBH in the NLAGNs (and possibly also in the TOs).

4.1. *Masses of SMBHs vs. accretion rates*

Our analysis of the NLAGNs in our sample is consistent with the standard AGN interpretation: this phenomenon is the product of the accretion of matter onto a SMBH that developed at the same time as the massive bulge of the galaxy. According to this interpretation, the nearby NLAGNs in our sample are possibly scaled-down (and/or powered-down) versions of quasars and broad-line AGNs (BLAGNs). One good example is our own galaxy, with an intermediate Sb or SBb morphology (Binney & Merrifield 1998), where evidence was found in its center for both a SBMH, with a mass of the order of 3 or $\sim 4\times10^6$ $M_\odot$ (Genzel & Townes 1987; Ghez, Morris, & Becklin 2000; Schödel, Merritt, & Eckart 2009), and of recent star formation episodes (Figer et al. 2004), which suggests it could be classified as a LINER or a TO by outside observers.

In Häring & Rix (2004) a strong correlation was found between bulge mass and black hole mass (see also Gültekin et al. 2009, and references therein). In Shemmer et al. (2004) and Matsuoka et al. (2011), a strong correlation was also found between the black hole mass and the gas metallicity. These two correlations are fully consistent with our observations: while the formation of the SMBH follows (or self-regulates) the formation of the bulge, the gas metallicity, being a product of the evolution of the stars, also depends on the bulge formation through typically high astration rates (Sandage 1986). Based on these observations, we may therefore expect the NLAGNs to follow the same correlations as the quasars and BLAGNs.

To calculate the black hole masses, $M_{\rm BH}$, as reported in Column 3 of Table 4, we used the relation between the bulge mass and black hole mass as determined by Häring & Rix (2004). For the isolated NLAGNs we find a median value of 4.8×10^6 $M_\odot$, which is two to three orders below the value found in BLAGNs, but in good agreement with the black hole mass found in the center of our galaxy (Genzel & Townes 1987; Ghez et al. 2000; Schödel et al. 2009).

In Figure 20 we compare the gas metallicities and black hole masses for the NLAGNs of our sample with those measured in quasars and BLAGNs (Shemmer et al. 2004). The metallicities measured by Shemmer et al. (2004) were transformed to the units used in our study by Neri-Larios et al. (2011). The NLAGNs seem to continue the linear correlation found for the quasars and BLAGNs in the lower metallicity regime. A linear fit with a correlation coefficient of $r_{\rm Pearson}=0.77$ and $r_{\rm Spearman}=0.83$, both with chance probability $P(r_{\rm Pearson})$ and $P(r_{\rm Spearman})$ practically equal to zero, suggests the metallicity increases with the black hole mass as:

$$\log([{\rm O/H}]) = -2.56 + 0.3590\times\log(M_{\rm BH})\,. \quad (6)$$

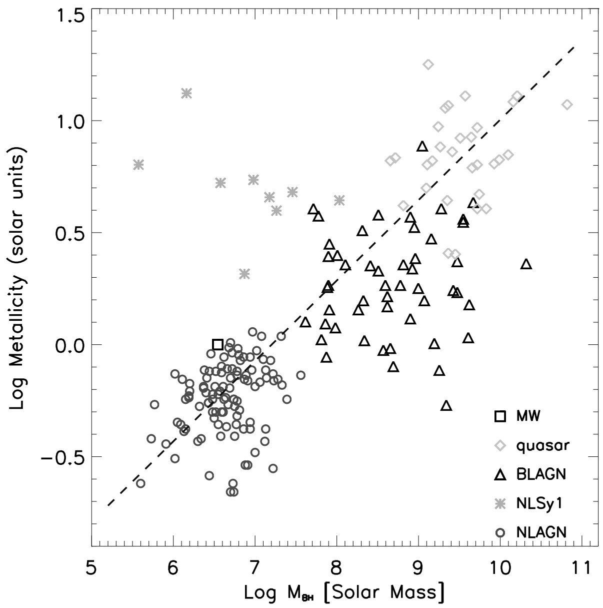

Fig. 20. Metallicities vs. black hole mass. The dashed line is our linear fitted correlation (excluding the NLSy1). The metallicity for the Milky Way is that of the Sun, which is now in better agreement with those of stars in its immediate neighborhood (Asplund et al. 2004). The color figure can be viewed online.

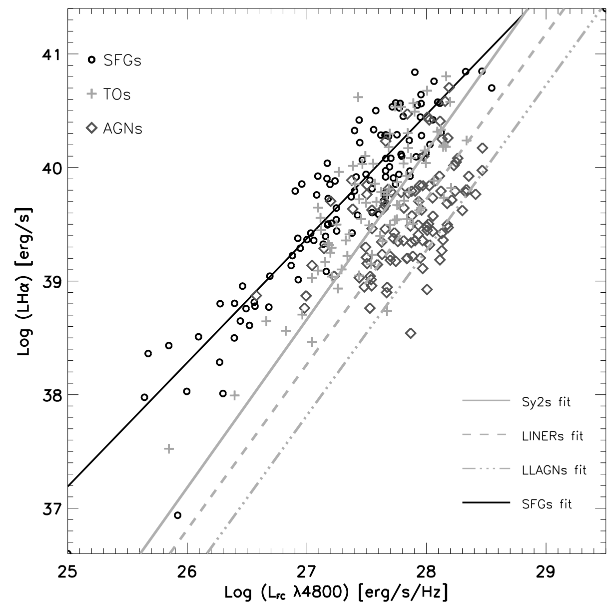

Fig. 21. Relation between ionization luminosity (Hα) and continuum luminosity (at 4800 Å). The different linear relations were determined by Torres-Papaqui et al. (2011) using a sample of 318486 SDSS galaxies. The SFGs follow a linear relation $L_{\mathrm{H}\alpha} \propto L_{4800}^{1.09\pm0.03}$, while the NLAGNs follow a steeper power law relation $L_{\mathrm{H}\alpha} \propto L_{4800}^{1.45\pm0.03}$. The color figure can be viewed online.

In Torres-Papaqui et al. (2011) it was shown that all the different kinds of NLAGNs (Seyfert 2, LINERS and LLAGNs) follow the same power law between the luminosity in Hα and luminosity at 4800 Å (Osterbrock 1989), while the SFGs follow a different, less steep, linear relation. In Figure 21 we verified that this also applies to the isolated NLAGNs of our sample. One can note also the intermediate position of the TOs, consistent with their being a mixture of SFGs and AGNs. This result suggests that we can use the black hole masses in conjunction with the luminosities at 5100 Å to estimate the accretion rates, as was done by Peterson et al. (2005).

In Figure 22, we follow the method of Peterson et al. (2005) to estimate the accretion rates of the NLAGNs of our sample. The SMBHs in the NLAGNs seem to accrete matter at relatively high rates of 0.1 times the Eddington limit. The isolated NLAGNs are consistent with scaled-down versions of quasars and BLAGNs, not powered-down versions: the lower luminosity is a result of smaller-mass black holes, not of lower accretion rates.

In Figure 23 we compare the gas metallicities and accretion rates of the NLAGNs of our sample with those found in quasars and BLAGNs, as determined in Neri-Larios et al. (2011) for the sample studied by Shemmer et al. (2004). Again, the NLAGNs seem to continue the linear correlation found for the quasars and BLAGNs in the lower metallicity regime. A linear fit with a correlation coefficient $r_{\mathrm{Pearson}} = r_{\mathrm{Spearman}} = 0.66$ with both chance probabilities practically equal to zero, suggests the metallicity increases with the accretion rate as:

$$\log([\mathrm{O/H}]) = 0.77 + 0.66 \times \log(L_{\mathrm{Bol}}/L_{\mathrm{Edd}})\,. \quad (7)$$

Although our results are fully consistent with the standard interpretation of NLAGNs as scaled-down versions of quasars and BLAGNs, we must state that there is an unfortunate uncertainty in the black hole masses we have determined. The fact is that there is no consensus in the literature about what is the correct relation to use. For practical reasons, we have used the relation proposed by Häring & Rix (2004) between the bulge mass and the black hole mass. However, in Gültekin et al. (2009) the relation proposed between black hole mass and velocity dispersion of the bulge yields masses which are ten times higher. The problem lies with what Häring & Rix (2004) called the "black hole sphere of influence". These authors argued that the black hole representing only a small fraction of the bulge mass (1% to

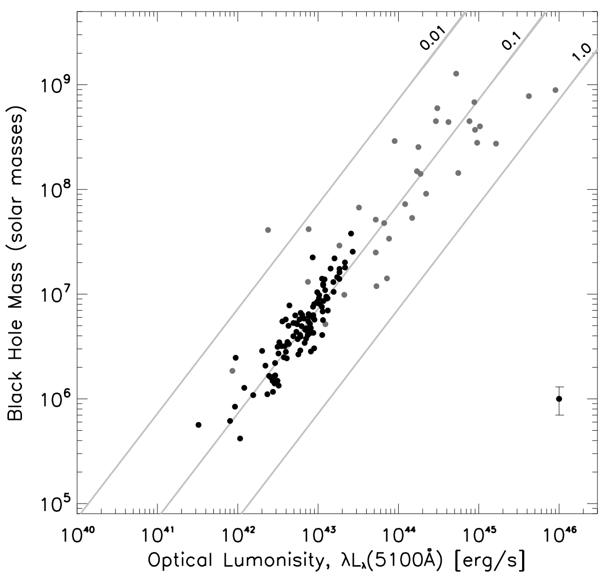

Fig. 22. Black hole mass as a function of continuum luminosity at 5100 Å for the NLAGNs compared to the BLAGNs studies in Peterson et al. (2005). The typical uncertainty for the NLAGNs is indicated by the red dot with error bars. The color figure can be viewed online.

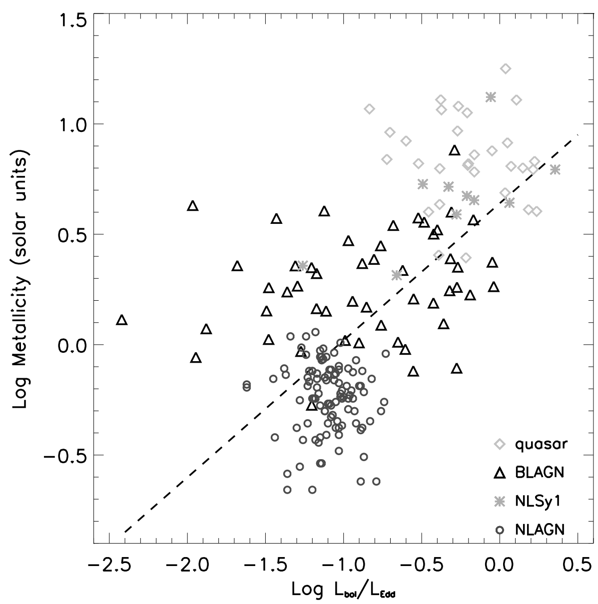

Fig. 23. Relation between metallicity and accretion rate. The NLAGNs are compared to the quasars and BLAGNs as studied by (Shemmer et al. 2004). The linear relation was fitted for all the galaxies (including the NLSy1). The color figure can be viewed online.

0.1%) cannot be responsible for the full value of the velocity dispersion, which explains why they apply a correction and obtain ten times smaller black hole mass values. In Gültekin et al. (2009), this correction is simply rejected as non valid, without further arguments.

If we adopt the relation of Gültekin et al. (2009), then the SMBH in the NLAGNs would be ten times more massive. In Figure 20, the relation between metallicity and black hole mass would be slightly steeper and the NLAGNs would differ significantly from the Milky Way. In Figure 22 the NLAGNs would not be scaled-down versions of BLAGNs but rather powered-down versions, that is, the SMBH of the NLAGNs would have masses comparable to those found in the BLAGNs but they would now be accreting at only 0.01 times the Eddington limit. Finally in Figure 23 the NLAGNs would fall farther to the left, but would still be in good agreement with the metallicity vs. accretion rate relation suggested by Shemmer et al. (2004).

5. SUMMARY AND CONCLUSION

We have constructed a sample of galaxies that have formed in low galactic density environments and have evolved in relative isolation. All these galaxies show a spiral disk and some kind of nuclear activity. Using a standard diagnostic diagram we have established that as many as 64% of these galaxies are classified as NLAGNs or TOs.

We have established a strong connection between the AGN phenomenon and the mass of the bulge, but have also found a strong correlation with the morphological type of the galaxies. This suggests that the AGN phenomenon is a "normal" occurrence related to the formation process of massive bulges in early-type spiral galaxies.

Consistent with this interpretation, our analysis suggests the AGNs and TOs have experienced during their formation higher astration rates than the SFGs–transforming their gas into stars more efficiently (Sandage 1986). Evidences favoring higher astration rates in AGNs than in SFGs are: (1) their older stellar populations; (2) their lower oxygen abundance and a possible excess of nitrogen. We also found the NLAGNs to have higher binding energies than the SFGs, suggesting they host a SMBH in their center.

Our results are in good agreement with the standard interpretation of NLAGNs, either as scaled-down (lower BH mass but same accretion rates) or powered-down (same BH mass but lower accretion rates) versions of quasars and BLAGNs. The NLAGNs also seem to follow the same relation between the BH mass, the accretion rate and the gas metallicity as the quasars and BLAGNs.

TABLE A1

DUNN'S POST TESTS FOR ACTIVITY TYPES VS. BULGE MASS, TOTAL MASS, METALLICITY AND GRAVITATIONAL BINDING ENERGY

	$M_{\rm Bulge}$		Group 1		Group 2		M_B		M_K		[O/H]		U/N	
	AGN	TO	AGN	TO	AGN	TO	AGN	TO	AGN	TO	AGN	TO	AGN	TO
AGN														
TO	***		ns		ns		ns		ns		***		***	
SFG	***	***	ns	ns	***	ns	***	**	***	***	***	***	***	**

We dedicate this article to the memory of Gabriel García Ruiz, night assistant and friend at the Observatorio Astronómico Nacional, San Pedro Mártir, Mexico, who died tragically while on duty at the end of 2010. The authors would also like to thank N. Bennert and S. Komossa for making their results of CLOUDY models available to us, and O. Shemmer for furnishing the data for the quasars and BLAGNs. T-P acknowledges PROMEP for support grant 103.5-10-4684 and I. P.-F. acknowledges a postdoctoral fellowship from Conacyt, Mexico No. 145727. This publication makes use of data products from the Two Micron All Sky Survey, which is a joint project of the University of Massachusetts and the Infrared Processing and Analysis Center/California Institute of Technology, funded by the National Aeronautics and Space Administration and the National Science Foundation. The SDSS is managed by the Astrophysical Research Consortium (ARC) for the Participating Institutions. The Participating Institutions are: the American Museum of Natural History, Astrophysical Institute Potsdam, University of Basel, University of Cambridge (Cambridge University), Case Western Reserve University, the University of Chicago, the Fermi National Accelerator Laboratory (Fermilab), the Institute for Advanced Study, the Japan Participation Group, the Johns Hopkins University, the Joint Institute for Nuclear Astrophysics, the Kavli Institute for Particle Astrophysics and Cosmology, the Korean Scientist Group, the Los Alamos National Laboratory, the Max-Planck-Institute for Astronomy (MPIA), the Max-Planck-Institute for Astrophysics (MPA), the New Mexico State University, the Ohio State University, the University of Pittsburgh, University of Portsmouth, Princeton University, the United States Naval Observatory, and the University of Washington.

APPENDIX – RESULTS OF STATISTICAL TEST

The statistical tests used in this study are the non-parametric Kruskal-Wallis test (KW), together with the Dunn's post tests. The KW test compares the medians in three or more unmatched groups of data and the post tests do multiple one-to-one comparisons. The P values reported in Tables A1 and A2 are codified in the following way: non significant difference, ns, significant, ** for $P < 0.01$, highly significant, *** for $P < 0.001$.

In Table A1, comparing the bulge mass in galaxies having different activity types, the post tests indicate that all three samples have different medians. In Group 1, no difference is found while in Group 2 only the AGNs differ from the SFGs.

In Table A2 we compare the bulge mass in galaxies having different morphologies; the post tests find highly significant differences between the most separated morphological classes. No differences are observed between the S0, S0a, Sa and Sab, the Sab and Sb, and the Sc and Sd. These tests suggest that the relation between bulge mass and activity type is a by-product of the morphology, consistent with the results for the diagnostic diagrams.

In Table A1 we verify that the total mass does not vary as strongly as the bulge mass in galaxies having different activity types. The same is true for the morphologies in Table A2. Therefore, the trend observed for the AGN activity is more qualitative than quantitative: it is not the mass of the galaxy that counts, but the fraction of mass that is in the form of a bulge.

In Table A1 we find significant differences in metallicities, the AGNs being less metal rich than the SFGs, and the TOs being intermediate. We also find a significant difference in metallicity between the early and late-type galaxies in Table A2, early-type galaxies being metal poor compared to late-type ones. These results are in good agreement with the difference in mean stellar population ages.

TABLE A2

DUNN'S POST TESTS FOR MORPHOLOGY VS. BULGE MASS, TOTAL MASS, METALLICITY AND GRAVITATIONAL BINDING ENERGY

	$M_{\rm Bulge}$					[O/H]				U/N				
	S0/S0a	Sa	Sab	Sb	Sc	S0/S0a	Sa	Sab	Sb	S0/S0a	Sa	Sab	Sb	Sc
Sa	ns					ns				ns				
Sab	ns	ns				ns	**			ns	***			
Sb	**	***	ns			**	***	ns		ns	***	ns		
Sc	***	***	***	**		***	***	***	ns	***	***	**	ns	
Sd	***	***	***	***	ns					***	***	***	***	ns

	M_B					M_K				
	S0/S0a	Sa	Sab	Sb	Sc	S0/S0a	Sa	Sab	Sb	Sc
Sa	ns					ns				
Sab	ns	ns				ns	ns			
Sb	ns	ns	ns			ns	**	ns		
Sc	**	**	ns	***		ns	***	ns	ns	
Sd	***	***	***	***	**	***	***	***	***	**

In Table A1 we find a strong relation between the gravitational binding energy and the AGN activity. This applies for galaxies having more massive bulges, Table A2. Since we find no such relation for the masses, these results are consistent with a strong dependence of the AGN phenomenon with the gravitational binding energy: the larger the gravitational binding energy, the larger the bulge mass and the higher the probability to find an AGN.

All these results favor an explanation in terms of astration rates: high astration rates produce massive bulges which increases the probability of finding an AGN.

REFERENCES

Abazajian, K. N., et al. 2009, ApJS, 182, 543
Aller, M. C., & Richstone, D. O. 2007, ApJ, 665, 120
Asari, N. V., et al. 2007, MNRAS, 381, 263
Asplund, M., Grevesse, N., Sauval, A. J., Allende Prieto, C., & Kiselman, D. 2004, A&A, 417, 751
Baldwin, J. A., Phillips, M. M., & Terlevich, R. 1981, PASP, 93, 5
Baskin, A., & Laor, A. 2005, MNRAS, 358, 1043
Bell, E. F., McIntosh, D. H., Katz, N., & Weinberg, M. D. 2003, ApJS, 149, 289
Bennert, N., Jungwiert, B., Komossa, S., Haas, M., & Chini, R. 2006, A&A, 446, 919
Binney, J., & Merrifield, M. 1998, Galactic Astronomy (Princeton: Princeton Univ. Press)
Blandford, R. D., Netzer, H., & Woltjer, L. 1990, Active Galactic Nuclei (Berlin: Springer-Verlag)
Blanton, M. R., & Roweis, S. 2007, AJ, 133, 734
Boisson, C., Joly, M., Moultaka, J., Pelat, D., & Serote Roos, M. 2000, A&A, 357, 850
Brodie, J. P., & Huchra, J. P. 1991, ApJ, 379, 157
Bruzual, G., & Charlot, S. 2003, MNRAS, 344, 1000
Chabrier, G. 2003, PASP, 115, 763
Cid Fernandes, R., Mateus, A., Sodré, L., Stasínska, G., & Gomes, J. M. 2005, MNRAS, 358, 363
Cooke, A. J., Baldwin, J. A., Ferland, G. J., Netzer, H., & Wilson, A. S. 2000, ApJS, 129, 517
Coziol, R. 1996, A&A, 309, 345
Coziol, R., Carlos Reyes, R. E., Considère, S., Davoust, E., & Contini, T. 1999, A&A, 345, 733
Coziol, R., Contini, T., Davoust, E., & Considère, S. 1998b, in ASP Conf. Ser. 147, Abundance Profiles: Diagnostic Tools for Galaxy History, ed. D. Friedli, M. Edmunds, C. Robert, & L. Drissen (San Francisco: ASP), 219
Coziol, R., Ribeiro, A. L. B., de Carvalho, R. R., & Capelato, H. V. 1998a, ApJ, 493, 563
Edmunds, M. G., & Pagel, B. E. P. 1984, MNRAS, 211, 507
Evans, I. N., & Dopita, M. A. 1985, ApJS, 58, 125
Faber, S. M., & Gallagher, J. S. 1979, ARA&A, 17, 135
Ferland, G. J., Korista, K. T., Verner, D. A., Ferguson, J. W., Kingdon, J. B., & Verner, E. M. 1998, PASP, 110, 761
Figer, D. F., Rich, R. M., Kim, S. S., Morris, M., & Serabyn, E. 2004, ApJ, 601, 319
Fukugita, M., Ichikawa, T., Gunn, J. E., Doi, M., Shimasaku, K., & Schneider, D. P. 1996, AJ, 111, 1748
Gavignaud, I., et al. 2008, A&A, 492, 637
Genzel, R., & Townes, C. H. 1987, ARA&A, 25, 377
Ghez, A. M., Morris, M., & Becklin, E. E. 2000, AGM, 16, 42

Gültekin, K., et al. 2009, ApJ, 698, 198
Hamann, F., & Ferland, G. 1993, ApJ, 418, 11
Häring, N., & Rix, H.-W. 2004, ApJ, 604, L89
Heckman, T. M. 1980, A&A, 87, 152
Jablonka, P., Martin, P., & Arimoto, N. 1996, AJ, 112, 1415
Jarrett, T. H., Chester, T., Cutri, R., Schneider, S., Skrutskie, M., & Huchra, J. P. 2000, AJ, 119, 2498
Karachentseva, V. E., Mitronova, S. N., Melnyk, O. V., & Karachentsev, I. D. 2010, Astrophys. Bull., 65, 1
Kauffmann, G., et al. 2003, MNRAS, 346, 1055
Kennicutt, R. C., Jr. 1992, ApJ, 388, 310
Kewley, L. J., Dopita, M. A., Sutherland, R. S., Heisler, C. A., & Trevena, J. 2001, ApJ, 556, 121
Kewley, L. J., Groves, B., Kauffmann, G., & Heckman, T. 2006, MNRAS, 372, 961
Kochanek, C. S., et al. 2001, ApJ, 560, 566
Krolik, J. H. 1999, Active Galactic Nuclei: from the Central Black Hole to the Galactic Environment (Princeton: Princeton Univ. Press)
Martínez, M. A., del Olmo, A., Coziol, R., & Focardi, P. 2008, ApJ, 678, L9
Martínez, M. A., del Olmo, A., Coziol, R., & Perea, J. 2010, AJ, 139, 1199
Matsuoka, K., Nagao, T., Marconi, A., Maiolino, R., & Taniguchi, Y. 2011, A&A, 527, 100
McCall, M. L., Rybski, P. M., & Shields, G. A. 1985, ApJS, 57, 1
Melnick, J., Terlevich, R., & Moles, M. 1986, in IAU Symp, 116, Luminous Stars and Associations in Galaxies, ed. C. W. H. DeLoore, A. Wilkis, & P. Laskarides (Dordrecht: Reidel), 505
Miller, C. J., Nichol, R. C., Gómez, P. L., Hopkins, A. M., & Bernardi, M. 2003, ApJ, 597, 142
Nagao, T., Maiolino, R., & Marconi, A. 2006, A&A, 447, 863
Neri-Larios, D. M., Coziol, R., Torres-Papaqui, J. P., Andernach, H., Islas-Islas, J. M., Plauchu-Frayn, I., & Ortega-Minakata, R. A. 2011, Narrow-Line Seyfert 1 Galaxies and their place in the Universe, ed. L. Foschini, M. Colpi, L. Gallo, D. Grupe, S. Komossa, K. Leighly, & S. Mathur (Trieste: PoS SISSA), id. 65 `http://pos.sissa.it/cgi-bin/reader/conf.cgi?confid=126`
Osterbrock, D. E. 1970, QJRAS, 11, 1990
__________. 1989, Astrophysics of Gaseous Nebulae and Active Galactic Nuclei (Mill Valley, CA: University Science Books)
Peterson, B. M., et al. 2005, ApJ, 632, 799
Phillips, M. M., Jenkins, C. R., Dopita, M. A., Sadler, E. M., & Binette, L. 1986, AJ, 91, 1062
Ramos Almeida, C., Pérez García, A. M., Acosta-Pulido, J. A., Rodríguez Espinosa, J. M., Barrena, R., & Manchado, A. 2006, ApJ, 645, 148
Richstone, D., et al. 1998, Nature, 395, 14
Roberts, M. S., & Haynes, M. P. 1994, ARA&A, 32, 115
Sandage, A. 1986, A&A, 161, 89
Schlegel, D. J., Finkbeiner, D. P., & Davis, M. 1998, ApJ, 500, 525
Schödel, R., Merritt, D., & Eckart, A. 2009, A&A, 502, 91
Shemmer, O., Netzer, H., Maiolino, R., Oliva, E., Croom, S., Corbett, E., & di Fabrizzio, L. 2004, ApJ, 614, 547
Storchi Bergmann, T. 1991, MNRAS, 249, 404
Storchi Bergmann, T., & Pastoriza, M. G. 1989, ApJ, 347, 195
Stoughton, C., et al. 2002, AJ, 123, 485
Struck-Marcell, C. 1981, MNRAS, 197, 487
Thurston, T. R., Edmunds, M. G., & Henry, R. B. C. 1996, MNRAS, 283, 990
Tinsley, B. M., & Larson, R. B. 1979, MNRAS, 186, 503
Torres-Papaqui, J. P., Coziol, R., Andernach, H., Islas-Islas, J. M., Ortega-Minakata, R. A., Neri-Larios, D. M., & Plauchu-Frayn, I. 2011, MNRAS, submitted
Turner, E. L., Aarseth, S. J., Blanchard, N. T., Mathieu, R. D., & Gott, J. R., III 1979, AJ, 228, 684
Ulrich, M.-H. J. 1971, ApJ, 163, 441
Vacca, W. D., & Conti, P. S. 1992, ApJ, 401, 543
van Zee, L., Salzer, J. J., Haynes, M. P., O'Donoghue, A. A., & Balonek, T. J. 1998, AJ, 116, 2805
Vazdekis, A., et al. 2010, MNRAS, 404, 1639
Veilleux, S., & Osterbrock, D. E. 1987, ApJS, 63, 295
Viegas, S. M., & de Gouveia dal Pino, E. M. 1992, ApJ, 384, 467
Wake, D. A., et al. 2004, ApJ, 610, L85
Weedman, D. W. 1986, Quasar Astronomy (Cambridge: Cambridge Univ. Press)
York, D. G., et al. 2000, AJ, 120, 1579
Younger, J. D., Hopkins, P. F., Cox, T. J., & Hernquist, L. 2008, ApJ, 686, 815
Zaritsky, D., Kennicutt, R. C., & Huchra, J. P. 1994, ApJ, 420, 87

H. Andernach, R. Coziol, J. M. Islas-Islas, D. M. Neri-Larios, R. A. Ortega-Minakata, and J. P. Torres-Papaqui: Departamento de Astronomía, Universidad de Guanajuato, Apdo. Postal 144, 36000 Guanajuato, Guanajuato, Mexico (heinz, coziol, jmislas, daniel, rene, papaqui@astro.ugto.mx).
I. Plauchu-Frayn: Instituto de Astrofísica de Andalucía (CSIC), E-18008, Granada, Spain (ilse@iaa.ee).